Biochemical Journal (2021) **478** 1023–1042
https://doi.org/10.1042/BCJ20200996

Research Article

Crystal structures of hydroxymethylbilane synthase complexed with a substrate analog: a single substrate-binding site for four consecutive condensation steps

Hideaki Sato[1], Masakazu Sugishima[1], Mai Tsukaguchi[1], Takahiro Masuko[2], Mikuru Iijima[3], Mitsunori Takano[3], Yoshiaki Omata[4], Kei Hirabayashi[5], Kei Wada[6], Yoshio Hisaeda[2] and Ken Yamamoto[1]

[1]Department of Medical Biochemistry, Kurume University School of Medicine, 67 Asahi-machi, Kurume 830-0011, Japan; [2]Department of Chemistry and Biochemistry, Graduate School of Engineering, Kyushu University, 744 Motooka, Nishi-ku, Fukuoka 819-0395, Japan; [3]Department of Pure and Applied Physics, School of Advanced Science and Engineering, Waseda University, 3-4-1 Okubo, Shinjuku-ku, Tokyo 169-8555, Japan; [4] Department of Molecular Biology, Faculty of Pharmaceutical Science, Yokohama University of Pharmacy, 601 Matano-cho, Totsuka-ku, Yokohama 245-0066, Japan; [5] Department of Applied Chemistry, Faculty of Science, Tokyo University of Science, 1-3 Kagurazaka, Shinjuku-ku, Tokyo 162-8601, Japan; [6]Department of Medical Sciences, University of Miyazaki, 5200 Kihara, Kiyotake, Miyazaki 889-1692, Japan

Correspondence: Hideaki Sato (hsato@med.kurume-u.ac.jp)

Hydroxymethylbilane synthase (HMBS), which is involved in the heme biosynthesis pathway, has a dipyrromethane cofactor and combines four porphobilinogen (PBG) molecules to form a linear tetrapyrrole, hydroxymethylbilane. Enzyme kinetic study of human HMBS using a PBG-derivative, 2-iodoporphobilinogen (2-I-PBG), exhibited noncompetitive inhibition with the inhibition constant being 5.4 ± 0.3 μM. To elucidate the reaction mechanism of HMBS in detail, crystal structure analysis of 2-I-PBG-bound holo-HMBS and its reaction intermediate possessing two PBG molecules (ES_2), and inhibitor-free ES_2 was performed at 2.40, 2.31, and 1.79 Å resolution, respectively. Their overall structures are similar to that of inhibitor-free holo-HMBS, and the differences are limited near the active site. In both 2-I-PBG-bound structures, 2-I-PBG is located near the terminus of the cofactor or the tetrapyrrole chain. The propionate group of 2-I-PBG interacts with the side chain of Arg173, and its acetate group is associated with the side chains of Arg26 and Ser28. Furthermore, the aminomethyl group and pyrrole nitrogen of 2-I-PBG form hydrogen bonds with the side chains of Gln34 and Asp99, respectively. These amino acid residues form a single substrate-binding site, where each of the four PBG molecules covalently binds to the cofactor (or oligopyrrole chain) consecutively, ultimately forming a hexapyrrole chain. Molecular dynamics simulation of the ES_2 intermediate suggested that the thermal fluctuation of the lid and cofactor-binding loops causes substrate recruitment and oligopyrrole chain shift needed for consecutive condensation. Finally, the hexapyrrole chain is hydrolyzed self-catalytically to produce hydroxymethylbilane.

Received: 17 December 2020
Revised: 10 February 2021
Accepted: 12 February 2021

Accepted Manuscript online: 12 February 2021
Version of Record published: 4 March 2021

Introduction

In animals, plants, and bacteria, the porphyrin biosynthesis pathway is essential and the formed cyclic tetrapyrrole, uroporphyrinogen III, is transformed to biological pigments such as hemes, chlorophylls, and cobalamin (Supplementary Figure S1) [1,2]. In porphyrin biosynthesis, hydroxymethylbilane synthase (HMBS, EC 2.5.1.61), also known as porphobilinogen deaminase, catalyzes the sequential condensation of four porphobilinogen (PBG) molecules to form a linear tetrapyrrole, hydroxymethylbilane (HMB), in the cytosol (Figure 1) [3,4]. This enzyme, which functions as a monomer, has dipyrrolmethane (DPM) as a unique cofactor in its active site, and a conserved cysteine residue of the enzyme (Cys261 in human HMBS) is covalently bound to the cofactor. HMBS proceeds

Biochemical Journal (2021) **478** 1023–1042
https://doi.org/10.1042/BCJ20200996

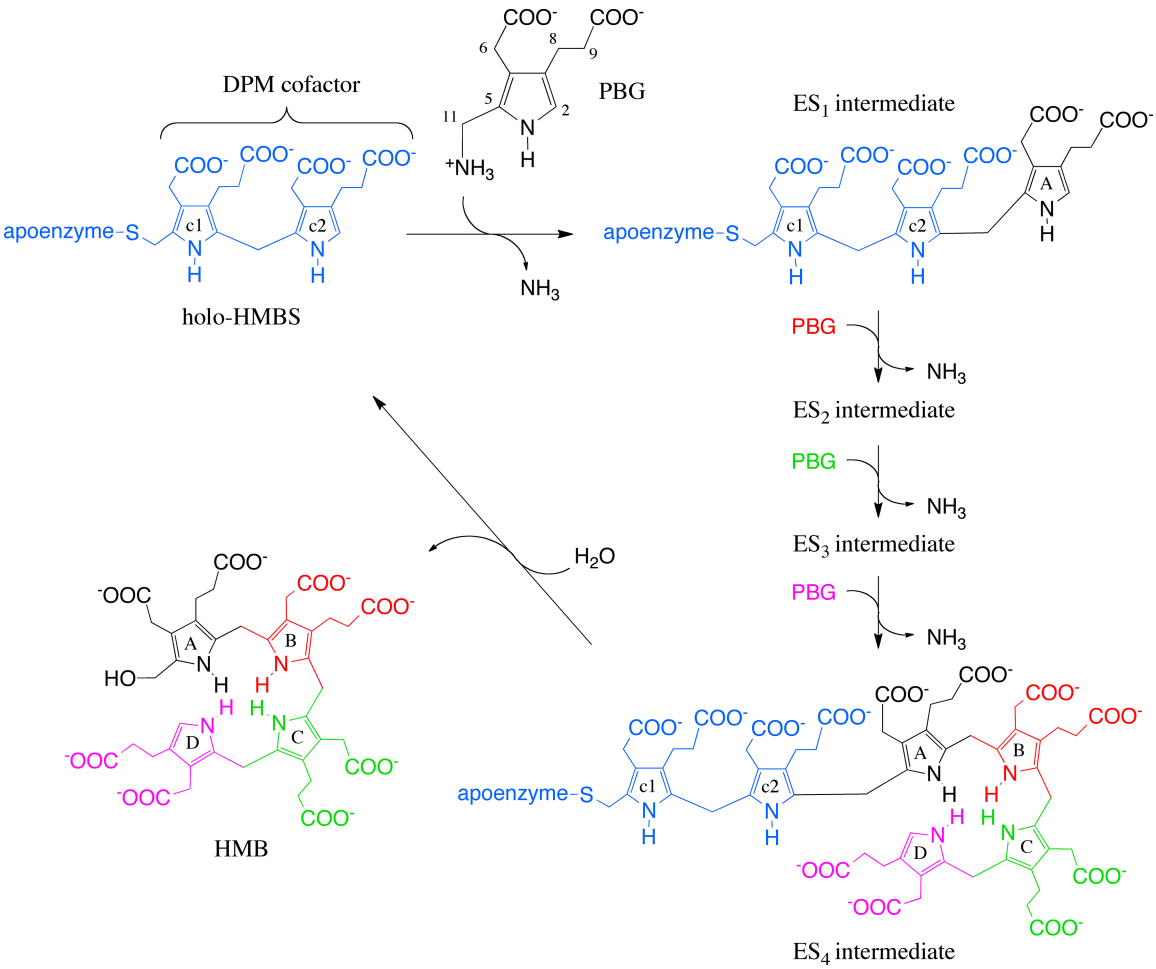

Figure 1. Reaction cycle of HMBS.

The DPM cofactor binds to apoenzyme via a thioether bond with the cysteine residue (Cys261 in human HMBS). Four molecules of the monopyrrole PBG are condensed to form a linear tetrapyrrole HMB with the elimination of four ammonia molecules by HMBS. Two pyrrole rings of the DPM cofactor and four rings for the tetrapyrrole product are denoted as c1, c2, A, B, C, and D from the cysteine residue side. The numbering of the atoms of PBG is also denoted.

by stepwise addition of pyrrolylmethyl groups until a linear hexapyrrole is formed in the active site. The four pyrrole rings of HMB are assembled on the DPM cofactor in the order of rings A, B, C, and D (Figure 1). Regarding the stepwise addition of pyrrole rings, it is still controversial whether the substrate-binding site is single or multiple [5,6]. The terminal tetrapyrrole is then hydrolyzed to yield the product HMB, leaving the cysteine-bound DPM cofactor on which assembly continues. Depending on the differences in promoters controlling transcription and alternative splicing, two isoforms of human HMBS are known: erythroid and non-erythroid (ubiquitous) isoforms. The ubiquitous isoform used in this study has additional 17 amino acid residues at the amino terminus. Uroporphyrinogen III synthase (EC 4.2.1.75) then cyclizes HMB by the rearrangement of ring D to yield uroporphyrinogen III (Supplementary Figure S1). In the absence of uroporphyrinogen III synthase, however, HMB cyclizes spontaneously to form uroporphyrinogen I. Ultimately, uroporphyrinogen III, but not uroporphyrinogen I, becomes heme through the biosynthesis pathway (Supplementary Figure S1).

The deficiency of activity of at least one enzyme in the heme biosynthesis pathway leads to a disease known as porphyria [7]. Insufficiency of protoheme causes the overexpression of 5-aminolevulinate synthase isoform 1 (ALAS1) and excessive accumulation and excretion of porphyrin precursors such as 5-aminolevulinic acid and PBG [1]. Particularly, lack of HMBS activity causes acute intermittent porphyria (AIP), which is the most

frequent type of porphyria. AIP is an autosomal dominant inherited disorder involved in heme biosynthesis, and its clinical symptoms include abdominal pain and neurological dysfunctions, but not cutaneous manifestations. More than 400 different gene mutations including missense, nonsense, deletion, and insertion related with human HMBS have been reported to date [8]. In order to discuss the causes of the reduced activity of these mutations leading to AIP, it is necessary to elucidate the detailed reaction mechanism of HMBS, including substrate binding, oligopyrrole chain elongation, and HMB release. For that purpose, it is indispensable to analyze the structure of intermediates formed during the enzymatic reaction.

Until date, the crystal structures of HMBS from humans [9,10], *Escherichia coli* [11,12], *Arabidopsis thaliana* [13], *Bacillus megaterium* [14], and *Vibrio cholerae* [15] have been determined as holoenzymes. All of them have a similar structure composed of three domains (domain 1, residues 1–116 and 216–239; domain 2, 117–215; domain 3, 240–361 in human HMBS) and possesses the DPM cofactor covalently attached to a conserved cysteine residue (Cys261 in human HMBS) in domain 3. The HMBS from *B. megaterium* has a partially oxidized cofactor, dipyrromethene or dipyrromethanone [14], and that from *A. thaliana* has another partially oxidized cofactor, dipyrromethenone [13]. It is considered that during the HMBS reaction, PBG binds to a putative substrate-binding site in the neighborhood of the distal pyrrole (c2) of the DPM cofactor in the cleft between domains 1 and 2. In human HMBS, an ordered sulfate ion derived from crystal mother liquor has been found at the proposed substrate-binding site, where Arg26 and Ser28 lie within hydrogen bonding distance to a substrate molecule [10]. This site is occupied by the propionate group of ring c2 of the oxidized cofactor in the *E. coli* HMBS [11]. The computational docking model of HMBS with some inhibitors has also predicted that the putative substrate-binding site accommodates the inhibitors [16]. Although the crystal structures of substrate(s)-bound HMBS had not been described for a few decades, Pluta et al. recently reported a crystal structure of a reaction intermediate (ES_2) of HMBS, which has a DPM cofactor covalently bound to two additional substrate pyrrole rings [16].

Some substrate derivatives such as 2-bromo-PBG [17,18], 9-fluoro-PBG (inhibition constant (K_i) = 6 μM, competitive inhibition) [19], and 6-methyl-PBG (K_i = 3 μM, mixed-type inhibition) [5] have been reported to be potent HMBS inhibitors. It has been observed by ^{13}C-NMR spectroscopy that 2-bromo-PBG binds covalently to the cofactor in the active site like PBG, and forms an enzyme–inhibitor complex [20]. The covalent attachment of 6-methyl-PBG to HMBS has been exhibited by Mono Q column chromatography and electrospray mass spectrometry analysis [5]. In addition, the 2-fluoro-11-hydroxy analog of PBG has been reported as a suicide inhibitor of HMBS, and its covalent bonding to HMBS has been shown by native polyacrylamide gel electrophoresis [21]. In contrast, 2-methyl-PBG is a weak competitive inhibitor of HMBS ($K_i \sim 1$ mM) [19]. The crystal structures of inhibitor-bound HMBS have not been reported until date.

In this study, the enzyme kinetics and crystal structure of HMBS were analyzed using 2-iodoporphobilinogen (2-I-PBG), a PBG-derivative, to detail the condensation mechanism of PBG molecules in the active site of HMBS. It was found that 2-I-PBG inhibits the HMBS reaction in a noncompetitive manner. Furthermore, we determined the crystal structures of the holo and ES_2 intermediate of HMBS in complex with 2-I-PBG. To the best of our knowledge, this is the first study to report the crystal structures of HMBS in complex with a substrate analog. The present structures of HMBS show a single substrate-binding site for four condensation reactions and provide clues to predict the mechanism of HMB detachment from the ES_4 intermediate of HMBS. In addition, molecular dynamics (MD) simulation of the ES_2 intermediate demonstrated characteristic thermal fluctuation of the lid loop and the cofactor-binding loop, which may induce substrate recruitment and shift of the oligopyrrole chain required for consecutive condensation in the single substrate-binding site.

Materials and methods

Materials

PBG was purchased from Frontier Scientific (Logan, UT, USA). All other chemicals used in this study were of reagent grade and obtained commercially.

Following the method described previously [22], 2-I-PBG was custom-synthesized by Mercachem (Nijmegen, The Netherlands). PBG (70 mg, 0.31 mmol) was suspended in 1 M acetate buffer (pH 4.6), and 0.5 M iodine in aqueous potassium iodide solution was added. The obtained compound was purified by dissolving it in diluted ammonia solution. This solution was neutralized with an aqueous acetic acid solution to pH 6, and the 2-I-PBG solid was filtered (59 mg, 0.17 mmol). LCMS-UV analysis showed a purity of 92%; ^{1}H-NMR (D_2O/DCl) δ 2.48 (t, 2H, –CH_2CH$_2$COOH), 2.65 (t, 2H, –CH$_2$CH_2COOH), 3.62 (s, 2H, –CH_2COOH), 4.11 (s, 2H,

Biochemical Journal (2021) 478 1023–1042
https://doi.org/10.1042/BCJ20200996

–CH_2NH_2); LCMS (negative) *m/z* 351 (100, $[M–H]^-$), 703 (81, $[2M–H]^-$); LCMS (positive) *m/z* 336 (100, $[M + H–NH_3]^+$), 705 (11, $[2M + H]^+$).

Expression and purification of holo form of HMBS (holo-HMBS)

The ubiquitous form of human HMBS was expressed in *E. coli* and purified as previously reported [23] with some modifications described below. Cells were lysed in and dialyzed after ammonium sulfate fractionation against 50 mM potassium phosphate buffer (pH 8.0). Gel filtration column chromatography was carried out using a HiLoad 26/600 Superdex 200 pg column (Cytiva; Uppsala, Sweden) in the same buffer. The HMBS-containing fractions were combined and diluted five-fold with cold distilled water and anion exchange column chromatography was performed with Whatman DE52 resin (Cytiva, 2.5 × 5 cm), as described previously [23].

Two additional column chromatography were carried out to obtain substrate-free holo-HMBS. The concentrated HMBS fraction was diluted 25-fold with 20 mM potassium phosphate buffer (pH 8.0) containing 1.0 M ammonium sulfate and applied to two 5-ml HiTrap Phenyl HP columns (Cytiva) connected in series equilibrated with the same buffer. After washing the column, the bound enzyme was eluted with a decreasing linear gradient of ammonium sulfate (1.0–0 M) in 20 mM potassium phosphate buffer (pH 8.0) at a flow rate of 1.0 ml/min. The HMBS-containing fractions were combined, concentrated, and desalted by ultrafiltration with Amicon Ultra-15 (Merck KGaA; Darmstadt, Germany). Finally, anion exchange column chromatography was performed with a Mono Q 4.6/100 PE column (Cytiva) equilibrated with 15 mM Tris–HCl buffer (pH 8.3) to remove the substrate(s)-bound intermediate forms of HMBS from cofactor-bound holo-HMBS [24]. After the column was washed with the same buffer, elution was achieved with a 60-ml linear gradient of NaCl (0–0.3 M) in the same buffer at a flow rate of 1.0 ml/min. Holo-HMBS-containing fractions were eluted at ca. 25 ml in a linear gradient and combined. Then, the obtained holo-HMBS solution was concentrated and desalted by ultrafiltration with Amicon Ultra-15 and stored at −80°C. The molecular weight of the purified holo-HMBS was confirmed by electrospray ionization time-of-flight mass spectrometry with a JMS-T100CS mass spectrometer (JEOL; Tokyo, Japan) (Calc. of holo-HMBS: 39617, Found: 39620; Supplementary Figure S2A).

Preparation of ES_2 intermediate of HMBS

To prepare a reaction intermediate of HMBS possessing two PBG molecules, ES_2 intermediate, 0.1 ml purified holo-HMBS (final conc. 4 μM) was mixed immediately with 15 ml PBG (final conc. 12 μM) in 15 mM Tris–HCl buffer (pH 8.3) on ice. The reaction mixture was concentrated by ultrafiltration with Amicon Ultra-15, filtrated with Ultrafree MC 0.22 μm filter (Merck KGaA), and applied to a Mono Q 4.6/100 PE anion exchange column equilibrated with 15 mM Tris–HCl buffer (pH 8.3). Subsequent washing and elution steps were carried out for holo-HMBS. Fractions containing the ES_2 intermediate eluted at ca. 31 ml in the linear gradient were combined, concentrated, and desalted by ultrafiltration with Amicon Ultra-15. For crystallization, the concentrated ES_2 intermediate was used immediately without freezing. The molecular weight of the ES_2 intermediate was confirmed by electrospray ionization time-of-flight mass spectrometry with a JMS-T100CS mass spectrometer (Calc. of the ES_2 intermediate: 40036, Found: 40039; Supplementary Figure S2B).

Enzyme kinetic study

HMBS activity was measured by optically quantifying the produced uroporphyrin [23,25]. The assay mixture (0.9 ml) comprising 0.1 M Tris-HCl buffer (pH 7.4), 0.1 mM dithiothreitol, 2 mg/ml bovine serum albumin, 16.4 nM holo-HMBS, 0–10 μM 2-I-PBG, and 0–500 μM PBG was incubated at 37°C for 30 min. The enzyme reaction was initiated by adding PBG and terminated by adding 0.1 ml 50% trichloroacetic acid. Enzymatically produced HMB cyclized to uroporphyrinogen I spontaneously (Supplementary Figure S1). To completely oxidize uroporphyrinogen I into uroporphyrin I, the sample solution was mixed with 0.4 ml 0.5% iodine–1% potassium iodide solution and incubated at 37°C for 5 min. To quench excess iodine, 0.1 ml 1% sodium disulfite solution was added to the sample solution and incubated at 37°C for 5 min. After removal of the precipitated protein by centrifugation, the amount of uroporphyrin in the supernatant was determined optically with a Shimadzu UV-2550 spectrophotometer (Kyoto, Japan) using a molar extinction coefficient (ε) of 528 mM^{-1} cm^{-1} at 406 nm [26]. As 2-I-PBG includes a trace amount of PBG as an impurity, a slight amount of uroporphyrin I was detected in the reaction mixture even without adding PBG. To analyze enzyme kinetics, this was

subtracted from the total amount of uroporphyrin I. The Cornish-Bowden method [27] was used to determine the inhibition type and the K_i value for 2-I-PBG.

Preparation of inhibitor-free and 2-I-PBG-bound holo-HMBS crystals

Human holo-HMBS was crystallized using the sitting drop vapor diffusion method. A 1-μl drop of holo-HMBS solution (ca. 11 mg/ml) in 15 mM Tris-HCl buffer (pH 8.3) containing 10 mM dithiothreitol was mixed with a 1-μl drop of reservoir solution comprising 0.20 M diammonium hydrogen citrate, 22% (w/v) PEG3350, and 10 mM dithiothreitol [9]. The sitting drops were equilibrated against 0.1 ml reservoir solution

Table 1. Crystallographic data collection and refinement statistics of human HMBS

	Inhibitor-free holo-HMBS	2-I-PBG-bound holo-HMBS	Inhibitor-free ES_2 intermediate	2-I-PBG-bound ES_2 intermediate
Data collection				
Wavelength (Å)	0.90	1.50 (f'' of iodine = 6.6)	0.90	1.50
Space group	$P2_12_12_1$	$P2_12_12_1$	$P2_12_12_1$	$P2_12_12_1$
Cell dimensions (Å)	a = 70.4, b = 80.8, c = 109.2	a = 73.9, b = 81.1, c = 109.0	a = 81.5, b = 79.5, c = 108.7	a = 81.4, b = 81.4, c = 108.9
Resolution[1] (Å)	43.1–1.84 (1.95–1.84)	48.9–2.40 (2.55–2.40)	45.2–1.79 (1.90–1.79)	45.2–2.31 (2.45–2.31)
R^2_{sym}	0.070 (0.452)	0.102 (0.623)	0.072 (1.081)	0.107 (0.566)
$I/\sigma I$	10.73 (2.31)	11.3 (2.8)	9.3 (1.3)	5.5 (1.5)
Completeness (%)	98.2 (92.0)	98.4 (95.4)	99.8 (99.2)	99.4 (97.2)
Redundancy	4.0 (2.8)	3.4 (3.4)	3.4 (3.4)	3.4 (3.2)
CC(1/2)	0.997 (0.915)	0.997 (0.851)	0.998 (0.688)	0.994 (0.901)
Refinement				
Resolution (Å)	43.1–1.84	48.9–2.4	45.2–1.79	45.2–2.31
No. reflections	53 343	25 902	66 528	32 254
R^3_{work}/R^4_{free}	0.19/0.25	0.20/0.27	0.20/0.24	0.23/0.28
No. atoms				
Protein	4747	4850	4900	4894
Coenzyme + substrates	60	60	120	120
Inhibitor	—	17	—	17
Water	159	64	368	76
B-factors				
Protein	48.9	40.8	34.7	57.7
Coenzyme + substrates	40.1	32.8	31.8	53.3
Inhibitor	—	40.9 (occupancy = 0.72)	—	60.6 (occupancy = 0.74)
Water	48.9	33.0	38.4	49.7
R.m.s. deviations				
Bond lengths (Å)	0.006	0.010	0.010	0.006
Bond angles (°)	0.745	1.319	1.217	1.011

[1]Values in parentheses refer to the highest resolution shell;
[2]$R_{sym} = \sum_{hkl}\sum_i|I_i(hkl) - \langle I(hkl)\rangle|/\sum_{hkl}\sum_i I_i(hkl)$;
[3]$R_{work} = \sum_{hkl}||F_o(hkl)| - |F_c(hkl)||/\sum_{hkl}|F_o(hkl)|$;
[4]R_{free} is the *R*-factor calculated for 5% of the data not included in the refinement.

Biochemical Journal (2021) 478 1023–1042
https://doi.org/10.1042/BCJ20200996

and incubated at 20°C for one week. Plate-shaped colorless single crystals of holo-HMBS were obtained (Supplementary Figure S3A). An inhibitor-free holo-HMBS crystal was picked up with a cryoloop and soaked in a cryoprotectant solution comprising 0.15 M ammonium citrate dibasic and 30% (w/v) PEG3350 at 25°C. To prepare a 2-I-PBG-bound holo-HMBS crystal, the holo-HMBS crystal was soaked in a cryoprotectant solution comprising 0.18 M triammonium citrate, 28% (w/v) PEG3350, 10 mM dithiothreitol, and 5 mM 2-I-PBG at 25°C for 2.5 min. Both crystals were flash-cooled and stored in liquid nitrogen until diffraction data were collected.

Preparation of crystals of inhibitor-free and 2-I-PBG-bound ES_2 intermediates

The ES_2 intermediate of HMBS was crystallized in a similar manner to the holo-HMBS and platy colorless single crystals of the inhibitor-free ES_2 intermediate formed within two days (Supplementary Figure S3B). An inhibitor-free ES_2 intermediate crystal was picked up with a cryoloop and soaked in a cryoprotectant solution comprising 0.20 M trisodium citrate, 26% (w/v) PEG3350, and 10 mM dithiothreitol at 25°C. To prepare 2-I-PBG-bound ES_2 intermediate crystals, inhibitor-free ES_2 intermediate crystals were grown under the same conditions, except they were grown anaerobically. After two weeks, a crystal was picked up with a cryoloop and soaked in a solution comprising 0.18 M trisodium citrate, 28% (w/v) PEG3350, 10 mM dithiothreitol, and 5 mM 2-I-PBG at 25°C for 2.5 min. Both prepared crystals were flash-cooled and stored in liquid nitrogen until diffraction data were collected.

Structure determination

Diffraction data of the inhibitor-free and 2-I-PBG-bound holo-HMBS and ES_2 intermediate crystals were collected at 100 K using synchrotron radiation ($\lambda = 1.50$ Å or 0.90 Å for 2-I-PBG-bound complexes or inhibitor-free enzymes, respectively) and the Rayonix MX225-HE detector (for the inhibitor-free and 2-I-PBG-bound holo-HMBS, and the inhibitor-free ES_2 intermediate) or Dectris EIGER X 16M detector (for the 2-I-PBG-bound ES_2 intermediate) at the BL44XU beamline of SPring-8 (Hyogo, Japan). Diffraction data were processed and scaled using XDS [28]. All crystals belonged to the space group $P2_12_12_1$ (Table 1). The HMBS structures were determined using the molecular replacement method with MolRep [29,30] and the human holo-HMBS structure (Protein Data Bank (PDB) accession code: 3ECR) [9] as a search model. The structure of the protein moiety and cofactor was refined with PHENIX [31] and manually adjusted with Coot [32]. For 2-I-PBG-bound forms, the resultant F_o–F_c electron density map showed significant electron density for 2-I-PBG. Anomalous difference Fourier map revealed the position of iodine atom. Then, 2-I-PBG was added to the model and refined. Finally, water molecules were added to the model and refined. The diffraction and refinement statistics are summarized in Table 1. The coordinates and structure factors of the inhibitor-free and 2-I-PBG-bound holo-HMBS and ES_2 intermediates were deposited in PDB with the accession codes 7CCX, 7CCY, 7CCZ, and 7CD0.

MD simulation of ES_2 intermediate

To examine the thermally activated internal motions of HMBS that should be relevant to the mechanism of substrate binding and oligopyrrole chain shifting, MD simulations were performed using the inhibitor-free ES_2 intermediate crystal structure. The disordered region in the lid loop (residues 58–75) was modeled by MODELLER [33] using the ordered region of the inhibitor-bound holo-HMBS lid loop. The disordered N-terminal tail (residues 1–18) was truncated. According to the protonation state evaluation by H++ [34], Glu223 was protonated and His160 was doubly protonated. The AMBER FF03 force field was used [35], and the atomic charges and other parameters for Cys261, to which the tetrapyrrole chain (composed of DPM and two PBGs) is covalently bonded, were generated by AM1-BCC [36] using antechamber [37] in combination with the GAFF force field [38]. HMBS was immersed in a truncated octahedral unit cell containing 10843 water molecules, 29 potassium ions, and 21 chloride ions. The whole system was initially equilibrated in the same way as in our previous study [39]. In the production run, multiple 0.7-μs-long simulations (16 independent simulations of total 11.2 μs) were conducted at isothermal (310 K) and isobaric (0.1 MPa) conditions. All MD simulations were conducted using AMBER14 [40].

Biochemical Journal (2021) **478** 1023–1042
https://doi.org/10.1042/BCJ20200996

Results

Enzyme kinetics

To evaluate the effect of the substrate analog 2-I-PBG in the HMBS reaction, the HMB formation rate was determined as the uroporphyrin I formation rate, which was calculated from absorbance changes at 406 nm. As shown in Figure 2, the Cornish–Bowden plot of the data showed convergent lines with an appropriate intersection, and exhibited that 2-I-PBG inhibited the HMBS reaction in a noncompetitive manner, with a K_i value of 5.4 ± 0.3 μM ($n = 4$). Reported competitive and mixed-type inhibitors, such as 2-bromo-PBG [17] and 6-methyl-PBG [5], respectively, form covalent bonds with the cofactor and oligopyrrole chain, while 2-I-PBG does not form as described below. This might indicate a difference in the inhibition of PBG analogs. As the K_i of 2-I-PBG is similar to that of some PBG analogs such as 6-methyl-PBG ($K_i = 3$ μM) [5] and 9-fluoro-PBG ($K_i = 6$ μM) [19], it should bind stably to the active site. Therefore, 2-I-PBG seemed to be suitable for crystal structure analysis of HMBS in complex with a substrate analog.

Crystal structure of 2-I-PBG-bound holo-HMBS

Although a crystal of 2-bromo-PBG-bound HMBS was unavailable for X-ray diffraction due to instability in an earlier investigation [17], we succeeded in preparing 2-I-PBG-bound enzyme crystals suitable for crystallography. A data set was collected to 2.40 Å resolution and the crystal of holo-HMBS in complex with 2-I-PBG belonged to the space group $P2_12_12_1$ with unit-cell parameters $a = 73.9$ Å, $b = 81.1$ Å, and $c = 109.0$ Å. There were two protein molecules in the asymmetric unit, and one of them included a 2-I-PBG molecule with an occupancy factor of 0.72. Data collection and refinement statistics are summarized in Table 1. The overall structure of the 2-I-PBG-bound holo-HMBS was found to be similar to that of the inhibitor-free holo-HMBS (Figure 3). In the 2-I-PBG-bound holo-HMBS, three domains and a DPM cofactor are conserved and Cys261 is covalently bound to the cofactor via a thioether bond. Although the two residues immediately before Cys261 were disordered in the previously reported holo-HMBS structure (PDB accession code: 3ECR) [9], they were ordered in the structures of 2-I-PBG-bound and inhibitor-free holo-HMBS determined in this study. As well as in the inhibitor-free holo-HMBS, numerous interactions between the DPM cofactor and protein moiety were observed in the 2-I-PBG-bound holo-HMBS (Table 2). For example, Ser96, Lys98, Asp99, Thr145, Ser147, Arg149, Arg150, and Arg173 participate in DPM cofactor binding. Compared to the present structure of inhibitor-free holo-HMBS, where a loop of residues 58–76 in domain 1 was disordered, the residues 58–69 were ordered in the 2-I-PBG-bound holo-HMBS structure (Figure 3C). Such flexibility of this loop in the proximity of the active site appears to be involved in the binding of 2-I-PBG and the substrate, although no direct interactions between the loop (residues 58–69) and 2-I-PBG were observed. Hereafter, this loop is called the lid loop.

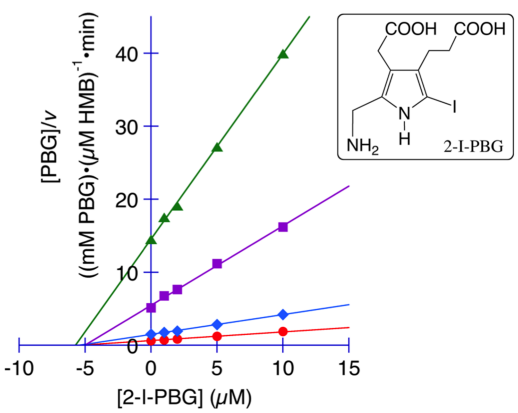

Figure 2. Enzyme kinetic study of HMBS with 2-I-PBG.

The reaction conditions are described in the Materials and Methods section. Data are shown in the Cornish–Bowden plot. The concentration of PBG was varied: 20 μM (circle), 50 μM (diamond), 200 μM (square), and 500 μM (triangle). The inset shows the structure of 2-I-PBG.

Biochemical Journal (2021) **478** 1023–1042
https://doi.org/10.1042/BCJ20200996

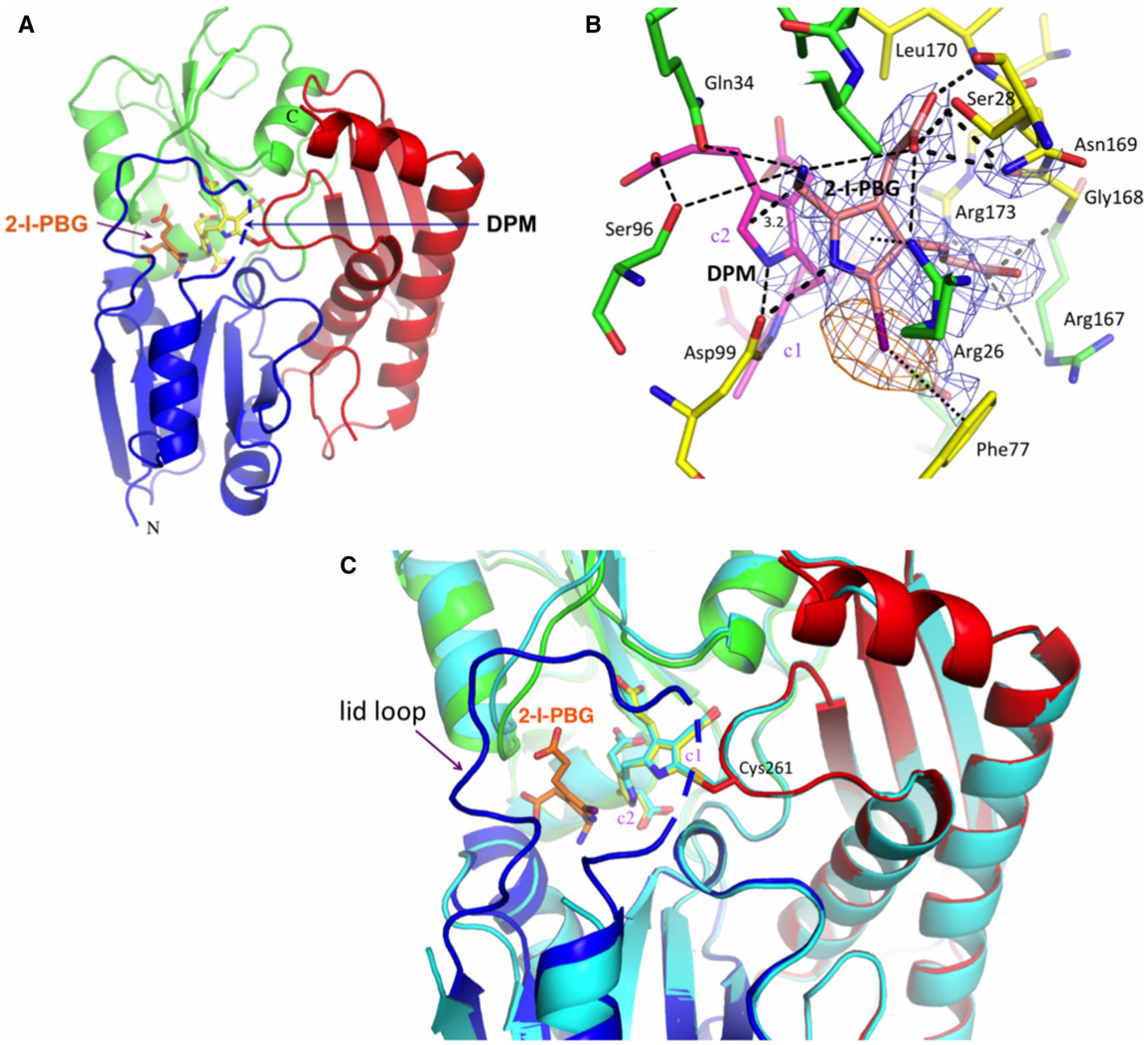

Figure 3. Crystal structure of human HMBS in complex with 2-I-PBG.

(**A**) Overall structure. Domains 1, 2, and 3 are displayed in blue, green, and red, respectively. The DPM cofactor and 2-I-PBG are shown as yellow and orange sticks, respectively. N and C termini of the protein are marked as N and C, respectively. Disordered region of the lid loop is shown in a broken line. (**B**) Active site. The omitted electron density map of 2-I-PBG is represented in blue mesh and contoured at 1.0 σ. Anomalous diffraction Fourier map is shown in orange mesh and contoured at 5.0 σ. The DPM cofactor and 2-I-PBG are shown in magenta and salmon-pink sticks, respectively. Iodine atom of 2-I-PBG is colored in purple. The two rings of the DPM cofactor are indicated as c1 and c2 from the side bound to Cys261. Several residues represented as sticks are forming ionic interactions and hydrogen bonds with 2-I-PBG. (**C**) Superimposition of 2-I-PBG-bound holo-HMBS (colored as in (**A**)) with the inhibitor-free holo-HMBS (colored in cyan). The rmsd of Cα atoms was 0.367 Å. Disordered region of the lid loop of 2-I-PBG-bound holo-HMBS is shown in a broken line.

As shown in Figure 3, the 2-I-PBG molecule is noncovalently bound to holo-HMBS at the proposed substrate-binding site in a cleft between domains 1 and 2. An anomalous peak was observed at the iodine atom of 2-I-PBG (Figure 3B). Binding of 2-I-PBG to holo-HMBS is stabilized by the following interactions (Table 2). The side chains of Ser28 and Asn169 and amide N of Leu170 form hydrogen bonds, and the side chain of Arg26 forms an ionic bond with the acetate group of 2-I-PBG. The side chain of Arg173 and amide N of Gly168 interact with the propionate group of 2-I-PBG through ionic and hydrogen bonds, respectively. The side chain of Arg167 may be associated with the propionate side chain of 2-I-PBG. Furthermore, the side chains of Gln34 and Ser96 form hydrogen bonds with the aminomethyl group of 2-I-PBG. The carboxy group of Asp99 also forms a hydrogen bond with the pyrrole N of 2-I-PBG. The pyrrole ring of 2-I-PBG shows

Biochemical Journal (2021) **478** 1023–1042
https://doi.org/10.1042/BCJ20200996

Table 2. Interactions between pyrroles and protein moiety in HMBS

	Inhibitor-free holo-HMBS	2-I-PBG-bound holo-HMBS	Inhibitor-free ES_2 intermediate	2-I-PBG-bound ES_2 intermediate
Substrate-binding site	—	*2-I-PBG* Acetate: Arg26 Acetate: Ser28 Acetate: Asn169 Acetate: Leu170 (>NH) Propionate: Arg173 Propionate: Gly168 (>NH) Propionate: Arg167 Aminomethyl: Gln34 Aminomethyl: Ser96 Aminomethyl: acetate of 2-I-PBG Pyrrole N: Asp99 Pyrrole ring: Arg26 Iodine: Phe77	—	*2-I-PBG* Acetate: Arg26 Acetate: Ser28 Acetate: Leu170 (>NH) Propionate: Arg173 Aminomethyl: Gln34 Pyrrole N: Asp99 Pyrrole ring: Arg26
Pyrrole-binding site 1	*ring c2* Acetate: Lys98 Acetate: Arg150 Acetate: Ala189 (>NH) Propionate: Ser96 Propionate: Arg195 Propionate: Gly218 (>NH) Pyrrole N: Asp99	*ring c2* Acetate: Lys98 Acetate: Arg150 Acetate: Ala189 (>NH) Propionate: Ser96 Propionate: Gly218 (>NH) Pyrrole N: Asp99	*ring B* Acetate: Lys98 Acetate: Arg150 Acetate: Ala189 (>NH) Propionate: Ser96 Propionate: Arg195 Propionate: Gly218 (>NH) Pyrrole N: Asp99	*ring B* Acetate: Lys98 Acetate: Arg150 Acetate: Ala189 (>NH) Propionate: Ser96 Propionate: Arg195 Propionate: Gly218 (>NH) Pyrrole N: Asp99
Pyrrole-binding site 2	*ring c1* Acetate: Lys98 Acetate: Ser147 Acetate: Arg149 Propionate: Arg150 Propionate: Arg173 Propionate: Ser146 (>NH) Pyrrole N: Asp99	*ring c1* Acetate: Lys98 Acetate: Ser147 Acetate: Arg149 Propionate: Arg150 Propionate: Arg173 Propionate: Thr145 Propionate: Ser146 (>NH) Pyrrole N: Asp99	*ring A* Acetate: Lys98 Acetate: Ser147 Acetate: Arg149 Propionate: Arg150 Propionate: Arg173 Propionate: Ser146 (>NH) Pyrrole N: Asp99	*ring A* Acetate: Lys98 Acetate: Ser147 Acetate: Arg149 Propionate: Arg150 Propionate: Arg173 Propionate: Thr145 Propionate: Ser146 (>NH) Pyrrole N: Asp99
Pyrrole-binding site 3	—	—	*ring c2* Acetate: Ser262 Pyrrole N: Lys98 (>C=O)	*ring c2* Acetate: Ser262 Acetate: pyrrole N of ring c1 Pyrrole N: Lys98 (>C=O)
Pyrrole-binding site 4	—	—	*ring c1* Acetate: Thr102 Acetate: Thr102 (>NH)	*ring c1* Acetate: Thr102 Acetate: Thr102 (>NH) Pyrrole N: acetate of ring c2

A schematic diagram of the substrate- and pyrrole-binding sites is depicted in Figure 7. Symbols of the pyrrole rings are shown in Figure 1. Interactions with the main chain are shown in parentheses.

face-to-face π–π stacking interaction with the distal pyrrole ring (c2) of the cofactor, and the distance between the two rings is 3.9 Å. Although the α-carbon of the pyrrole ring c2 of DPM is close to the aminomethyl carbon of 2-I-PBG, the distance between two carbon atoms (3.2 Å) is too long to form a covalent bond. A

Biochemical Journal (2021) **478** 1023–1042
https://doi.org/10.1042/BCJ20200996

cation–π interaction [41] between the side chain of Arg26 and the pyrrole ring of 2-I-PBG (=N^+H_2 – ring: 3.6 Å) and a face-on type halogen–π interaction between the iodine atom of the inhibitor and the aromatic ring of Phe77 (–I – ring: 3.7 Å) were also observed. Among the reported PBG-derivative HMBS inhibitors, 2-methyl-PBG shows unusually weak competitive inhibition (K_i = ca. 1 mM) [19]. The absence of the halogen–π interaction for 2-methyl-PBG could cause the high K_i value.

Crystal structure and MD simulation of inhibitor-free ES_2 intermediate

The inhibitor-free ES_2 intermediate structure was determined at 1.79 Å resolution and it was confirmed that two PBG molecules were covalently bound to the DPM cofactor in the active site (Figure 4). Compared to the substrate-free holo-HMBS, the substrate-derived dipyrrole is located in the space originally occupied by the DPM cofactor, and the DPM cofactor and a cofactor-binding loop including Cys261 moves backward (Figure 4C, Table 2). The side chain and amide N of Thr102 interacts with the acetate group of ring c1

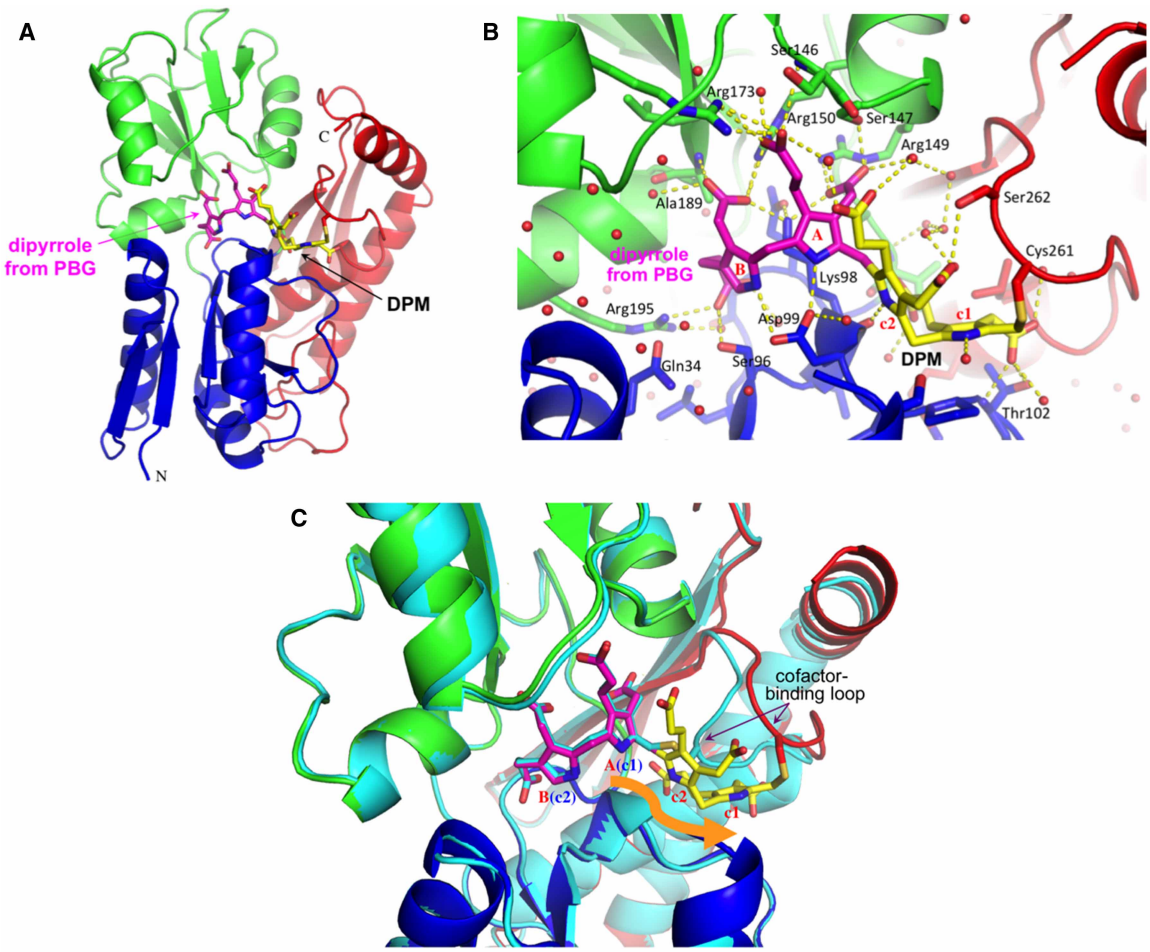

Figure 4. Crystal structure of inhibitor-free ES_2 intermediate of HMBS.

Domains 1, 2, and 3 of the ES_2 intermediate are indicated in blue, green, and red, respectively. The DPM cofactor and a covalently bound dipyrrole derived from two PBG molecules are shown as yellow and magenta sticks, respectively. (**A**) Overall structure. The N and C termini of the protein are marked as N and C, respectively. (**B**) Close-up view of the active site. Dotted lines indicate ionic and hydrogen bonds. Water molecules were drawn as red spheres. Two pyrrole rings of the DPM cofactor and two pyrrole rings from the PBG molecules in the tetrapyrrole chain are denoted as c1, c2, A, and B from the Cys261-connecting side. (**C**) Superimposition of inhibitor-free ES_2 intermediate with inhibitor-free holo-HMBS (cyan). The rmsd of the Cα atoms was 0.206 Å. Direction of movement of the DPM cofactor and the cofactor-binding loop in the ES_2 intermediate during oligopyrrole chain elongation is indicated by an orange arrow.

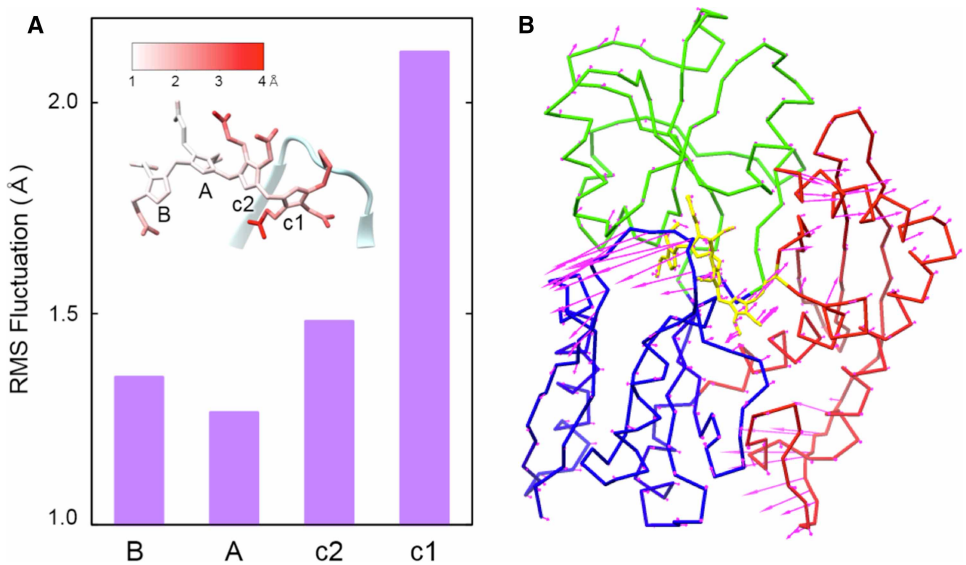

Figure 5. Thermal fluctuation of tetrapyrrole chain and HMBS.

(**A**) Root mean square fluctuation (RMSF) of each pyrrole ring in the tetrapyrrole chain. The RMSF value is the average of the five heavy atoms in each pyrrole ring. The RMFS values for individual atoms including those in the propionate and acetate groups are displayed in the inset. (**B**) The direction of the collective motion of HMBS obtained from the principal component analysis of the thermal fluctuation is shown by the set of arrows (magenta), which represents the second largest principal mode (eigenvector). Domains 1, 2, and 3 are indicated in blue, green, and red, respectively. The tetrapyrrole chain is shown as yellow sticks.

(Figure 4B). Further, the side chain of Ser262 interacts with the acetate group of ring c2, and carbonyl O of Lys98 associates with pyrrole N of ring c2. These results suggest that the linkage of one PBG molecule to the oligopyrrole chain of the HMBS reaction intermediate causes a shift in the chain by one pyrrole unit at each stage of the catalytic reaction.

MD simulation of the ES_2 intermediate demonstrates that the pyrrole rings of the two PBGs in the tetrapyrrole chain (particularly ring A) are strongly bound to HMBS and immobilized (Figure 5A) because of extensive electrostatic interactions between the negative charges in the acetate/propionate groups of PBG and the positive charges in the surrounding basic residues of HMBS (Supplementary Movie S1). In particular, five arginine residues in domain 2 (Arg149, Arg150, Arg167, Arg173, and Arg195) contribute largely to the strong positive electrostatic surface potential of the PBG-binding region (Supplementary Figure S4). In contrast, the pyrrole rings of DPM are mobile (Figure 5A) and partially stabilized by lysine residues in the lid loop (Lys70, Lys74, and Lys79) and arginine residues in domain 3 (Arg251, Arg255, and Arg355) that form intermittent electrostatic interactions with the acetate/propionate groups of DPM (Supplementary Movie S2). Intermittent hydrogen bonding between Ser262 and the acetate/propionate groups of DPM was also observed. The principal component analysis of the thermal fluctuation of the ES_2 intermediate shows that the lid loop, the cofactor-binding loop, and the insertion region (residues 296–324, not present in bacterial HMBS) fluctuate largely in a collective manner (Figure 5B and Supplementary Movie S3). The cofactor-binding loop moves in the direction that pulls the DPM from the binding site, even though the shift of the tetrapyrrole chain was not observed due to the strongly bound PBGs. The lid loop exhibits a large-amplitude open-close motion, and a short-lived helix formation is occasionally observed, reflecting its helix-forming propensity [16]. The possible roles of these characteristic thermal motions will be discussed later.

2-I-PBG-bound ES_2 intermediate structure

The crystal structure of the ES_2 intermediate in complex with 2-I-PBG was also determined at 2.31 Å resolution (Figure 6). Two protein molecules were observed in the asymmetric unit, and one of them had a 2-I-PBG molecule with an occupancy factor of 0.74. Data collection and refinement statistics are summarized in Table 1.

Biochemical Journal (2021) **478** 1023–1042
https://doi.org/10.1042/BCJ20200996

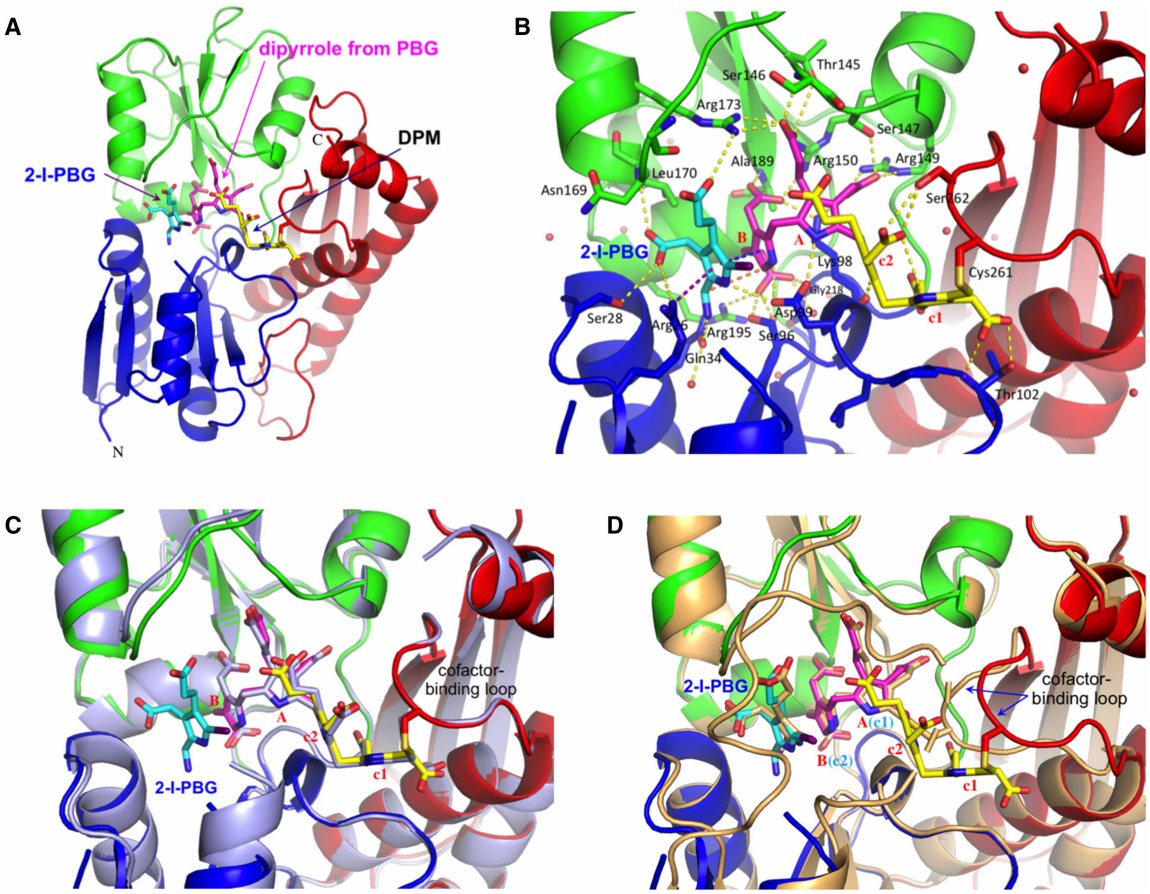

Figure 6. Crystal structure of ES_2 intermediate in complex with 2-I-PBG.

Domains 1, 2, and 3 of the 2-I-PBG-bound ES_2 intermediate are indicated in blue, green, and red, respectively. The DPM cofactor, a covalently bound dipyrrole derived from two PBG molecules, and 2-I-PBG are shown in yellow, magenta, and cyan sticks, respectively. (**A**) Overall structure. The N and C termini of the protein are marked as N and C, respectively. (**B**) Close-up view of the active site. The pyrrole rings of the tetrapyrrole chain are denoted as c1, c2, A, and B from the Cys261-connecting side. Several peripheral residues represented as sticks form ionic interactions and hydrogen bonds with the tetrapyrrole chain and 2-I-PBG (yellow dotted line). Focusing on 2-I-PBG, a π–π stacking interaction, cation–π interaction, and pyrrole α-C–aminomethyl C distance are indicated by dotted lines colored in blue, purple, and orange, respectively. (**C**) Superimposition of the 2-I-PBG-bound ES_2 intermediate with the inhibitor-free ES_2 intermediate (light blue). The rmsd of the Cα atoms was 0.452 Å. (**D**) Superimposition of the 2-I-PBG-bound ES_2 intermediate with the 2-I-PBG-bound holo-HMBS (light orange). The rmsd of the Cα atoms was 0.322 Å.

Except for the PBG analog, the overall 2-I-PBG-bound ES_2 intermediate structure was similar to that of the inhibitor-free ES_2 intermediate (Figure 6C). In the 2-I-PBG-bound ES_2 intermediate, three domains and a DPM cofactor linked to dipyrrole derived from two PBG molecules were found, and Cys261 was covalently bound to the cofactor via a thioether bond. Similar to the structure of the inhibitor-free ES_2 intermediate, the residues 58–76 of the lid loop in domain 1 are disordered in the 2-I-PBG-bound ES_2 intermediate.

In the structure of the 2-I-PBG-bound ES_2 intermediate, 2-I-PBG was observed close to the terminus of a tetrapyrrole chain, which was formed by the DPM cofactor and two PBG molecules, at the proposed substrate-binding site in a cleft between domains 1 and 2 (Figure 6B). This corresponds to the situation where the third substrate molecule is condensed to the tetrapyrrole chain in HMBS, becoming the ES_3 intermediate. A 2-I-PBG molecule was bound to the ES_2 intermediate by the following interactions (Table 2). The side chains of Arg26 and Ser28 form ionic and hydrogen bonds with the acetate group of 2-I-PBG, respectively. Amide N of Leu170 also forms a hydrogen bond with the acetate group. The side chain of Arg173 forms an ionic bond with the

propionate group of 2-I-PBG. Arg173 also forms an ionic bond with the propionate group of ring A of the tetrapyrrole chain. The side chain of Gln34 shows a hydrogen bond with the aminomethyl group of 2-I-PBG. The carboxy group of Asp99 forms hydrogen bonds with the pyrrole N of 2-I-PBG and both pyrrole nitrogens of rings A and B of the tetrapyrrole. However, Asp99 does not interact with either ring c1 or c2 of the cofactor. The pyrrole ring of 2-I-PBG showed a face-to-face π–π stacking interaction with the terminal pyrrole ring B of the tetrapyrrole chain, and the distance between these two rings was 4.0 Å (Figure 6B). A cation–π interaction [41] between the side chain of Arg26 and the pyrrole ring of 2-I-PBG was also observed (=N^+H_2 – ring: 4.2 Å). Therefore, in the 2-I-PBG-bound ES_2 intermediate structure, numerous bonds and interactions contribute to the binding of 2-I-PBG in the neighborhood of the terminal pyrrole B of the tetrapyrrole chain. However, the average temperature factor of 2-I-PBG in the 2-I-PBG-bound ES_2 intermediate was relatively higher than that in the 2-I-PBG-bound holo-HMBS (Table 1), indicating that the binding of 2-I-PBG to the ES_2 intermediate is relatively unstable. Unlike 2-I-PBG-bound holo-HMBS structure, a face-on type halogen–π interaction between iodine atom of the inhibitor and aromatic ring of Phe77 was not observed, which might cause the unstable binding of 2-I-PBG to the ES_2 intermediate. Furthermore, we also attempted crystallization and structure analysis of ES_3 intermediate of HMBS, and successfully obtained its crystals. However, structural analysis of ES_3 intermediate has not yet been successful due to its instability.

Discussion

Substrate-binding site and HMBS mutants in patients with AIP

Both structures of HMBS in complex with the substrate analog 2-I-PBG revealed in this study suggest the presence of a single substrate-binding site close to the terminal pyrrole of the DPM cofactor in holo-HMBS (Figure 6D). In both 2-I-PBG-bound HMBS structures, the negatively charged carboxy groups of 2-I-PBG interact with positively charged (Arg26, Arg173, and Arg167) and polar amino acid residues (Ser28, Gln34, Ser96, and Asn169) in the substrate-binding site (Table 2, Figure 7). In addition, the side chain of Asp99 and amide nitrogens of Leu170 and Gly168 are involved in 2-I-PBG binding.

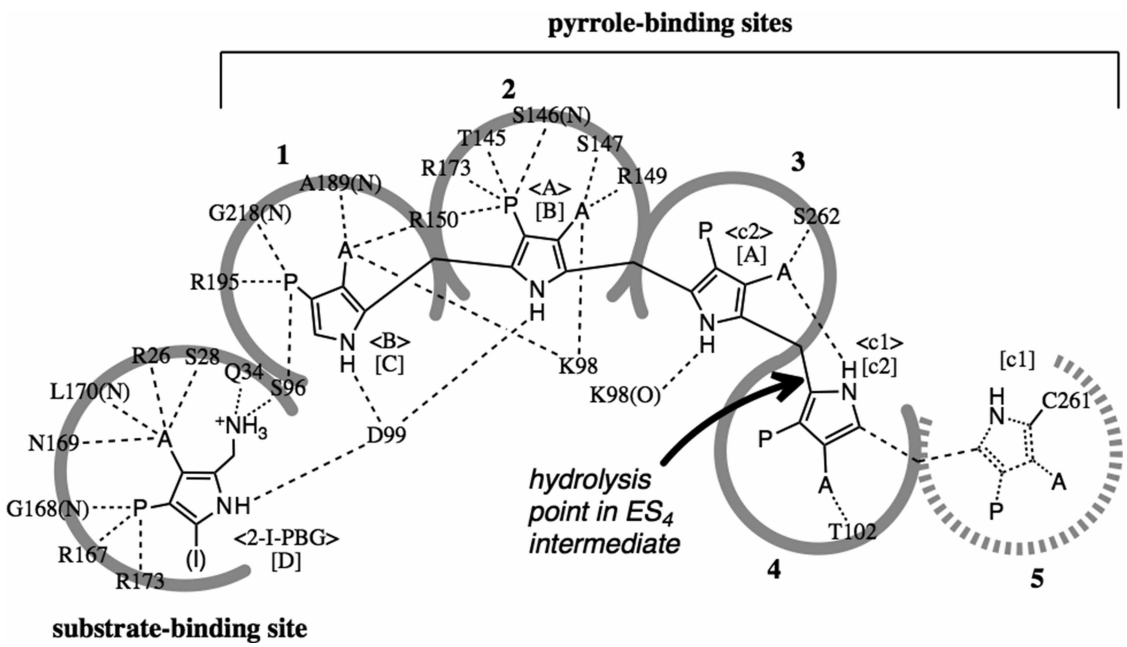

Figure 7. Schematic diagram of substrate- and pyrrole-binding sites in HMBS.

Interactions between pyrroles and peripheral residues are shown by broken lines. Acetate and propionate side chains are indicated as –A and –P, respectively. The pyrrole-binding site 5 cannot be determined from the present crystal structures. For the 2-I-PBG-bound ES_2 intermediate and the assumed ES_4 intermediate, the symbols for each ring are shown in angle brackets and square brackets, respectively.

Biochemical Journal (2021) **478** 1023–1042
https://doi.org/10.1042/BCJ20200996

Arg26 is a well conserved residue across species with available sequence data [10] and contributes to salt bridge and cation–π interaction with acetate side chain and pyrrole ring of 2-I-PBG, respectively (Figures 3B, 6B). In the patients with AIP, Arg26Cys (0.3% residual activity) [42] and Arg26His (0.2%) [43] mutants have been reported [44]. Arg26Ala mutation also has showed inactivation [9]. Furthermore, Arg26 in human HMBS corresponds to Arg11 in *E. coli* enzyme, and Arg11Leu (1.4% residual activity) [45] and Arg11His (3.9%) [46] mutants of *E. coli* HMBS show little activity. In the reaction intermediate separation assay using Mono Q column chromatography, no enzyme–substrate complex has been detected for the *E. coli* Arg11His mutant [47]. Therefore, Arg26 is particularly important for substrate binding, and its mutations lead to the loss of the ionic interaction with the acetate group of the substrate PBG, resulting in enzymatic activity reduction.

Ser28 is also highly conserved across species [10] and contributes to the hydrogen bond with the acetate group of 2-I-PBG in both 2-I-PBG-bound HMBS structures (Figures 3B, 6B). Ser28Asn mutant has been found in the patients with AIP [48] and has a low activity (0.8% residual activity [6]). Thus, it is suggested that Ser28 participates in substrate binding, and that loss of substrate binding to the substrate-binding site caused by its mutation results in reduced enzyme activity. The side chain of Gln34 forms a hydrogen bond with the amino-methyl group of 2-I-PBG in both inhibitor-bound structures (Figures 3B, 6B). Gln34 is a highly conserved residue across species [10], and it is known that Gln34Arg (0.7% residual activity) and Gln34Lys (0.2%) mutants reported in the patients with AIP are inactive [6]. It is suggested that Gln34 is involved in substrate binding and promotes the deamination of PBG in the HMBS reaction. In the 2-I-PBG-bound holo-HMBS structure, the side chain of Ser96 participates in hydrogen bonds with the aminomethyl group of 2-I-PBG as well as the propionate group of ring c2 of the DPM cofactor (Figure 3B). The Ser96Phe mutant has been reported in the patients with AIP [49]. Thus, Ser96 may contribute to not only cofactor binding, but also substrate binding at the appropriate position.

In both 2-I-PBG-bound structures, the side chain of Arg173 forms a salt bridge with the propionate groups of 2-I-PBG and the second pyrrole from the terminal of the oligopyrrole chain (ring c1 of the 2-I-PBG-bound holo-HMBS or ring A of the 2-I-PBG-bound ES_2 intermediate) (Figure 6B). Arg173 is also well conserved across species [10], and the Arg173Trp mutant in the patients with AIP has been reported to be inactive because of the absence of the cofactor [50,51]. In addition, Arg173Gln mutant (0.6% [52] or 0.15% residual activity [44]) found in the patients with AIP is inactive due to the absence of the cofactor [53]. Arg173 in human HMBS corresponds to Arg155 in the *E. coli* enzyme, and Arg155Leu (0.3% residual activity) [45] and Arg155His (1%) [47] mutants of *E. coli* HMBS are known to be inactive. In the reaction intermediate separation assay using Mono Q column chromatography with high PBG concentration (200 μM), Arg155Leu and Arg155His mutants accumulated ES_1 and ES_3 intermediates, respectively [47]. Thus, Arg173 should be important for not only stabilization of cofactor binding, but also PBG binding to the substrate-binding site.

Based on the structures of 2-I-PBG-bound HMBS, a loop consisting of residues 164–170 in domain 2 might contribute to not only inhibitor binding, but also substrate binding. Upon binding of 2-I-PBG to holo-HMBS, the side chain of Arg167 flipped largely and interacted weakly with the propionate group of the inhibitor (Figure 3B). In the case of the 2-I-PBG-bound ES_2 intermediate structure, however, the side chain of Arg167 was not clear due to disorder. Arg167 is highly conserved across species [10], and Arg167Trp [54] (2.3% residual activity [6]) and Arg167Gln (1.0% [6] or 0.7% [52]) mutants reported in the patients with AIP have little activity. In the previously reported crystal structure of the Arg167Gln mutant, the electron density of the side chain of the glutamine residue at 167 position had poor resolution [10]. Such substitutions of Arg167 might hamper substrate binding at the appropriate position. The side chain of Asn169 participated in hydrogen bonding with the acetate group of the inhibitor in the 2-I-PBG-bound holo-HMBS (Figure 3B), whereas Asn169 and 2-I-PBG appeared to be distant in the 2-I-PBG-bound ES_2 intermediate (Figure 6B). Until date, no mutation of this residue has been identified in the patients with AIP. Therefore, the significance of Asn169 for substrate binding in the active site might be limited, although it is well conserved across species [10]. In the 2-I-PBG-bound holo-HMBS structure, the amide N of Gly168 interacted with the propionate group of 2-I-PBG through hydrogen bonding. In addition, the hydrogen bond between amide N of Leu170 and the acetate group of 2-I-PBG contributed to the binding of the substrate analog. Therefore, it is suggested that the loop consisting of residues 164–170 would be useful to keep a substrate molecule at a proper position in the substrate-binding site for subsequent condensation.

Moreover, Asp99 is a catalytically important residue in HMBS and is well conserved across species with available sequence data [10]. The carboxy group of Asp99 forms hydrogen bonds with the pyrrole nitrogen of 2-I-PBG and terminal two pyrrole nitrogens of the oligopyrrole chain (rings c1 and c2 of the 2-I-PBG-bound

holo-HMBS, or rings A and B of the 2-I-PBG-bound ES_2 intermediate) (Figures 3B, 6B). In the patients with AIP, it has been shown that Asp99Gly [55] (3.2% residual activity [6]), Asp99His [56] (3.3% [6]), and Asp99Asn mutants [57] are inactive. Asp99 in human HMBS corresponds to Asp84 in the *E. coli* enzyme. It has also been reported that the Asp84Glu mutant of *E. coli* HMBS retains less than 1% activity, while forming highly stable enzyme-intermediate complexes [58]. Further, it has been known that Asp84Ala and Asp84Asn mutants of *E. coli* HMBS cannot catalyze HMB formation, although they appear to assemble the DPM cofactor [58]. Therefore, Asp99 in human HMBS promotes cofactor assembly, 2-I-PBG (also substrate) binding, and substrate condensation. As a substrate-binding site, a pocket composed of the residues involved in the inhibitor binding, such as Arg26, Ser28, Gln34, Ser96, Arg173, Arg167, Asn169, and Asp99, should accept the substrate.

In the present crystal structures of 2-I-PBG-bound HMBS, the aminomethyl group of 2-I-PBG was found in the neighborhood of the terminal pyrrole ring (c2 or B) of the oligopyrrole chain, but no covalent linkage was observed between the inhibitor and the terminal pyrrole ring. The distances between aminomethyl carbon atom of 2-I-PBG and α-carbon atom of the terminal pyrrole of the chain were 3.2 Å in the 2-I-PBG-bound holo-HMBS (Figure 3B) and 4.0 Å in the 2-I-PBG-bound ES_2 intermediate (Figure 6B). These results are consistent with the fact that a covalently 2-I-PBG-bound holo-HMBS was not detected by electrospray ionization time-of-flight mass spectrometry analysis. In contrast to 2-bromo-PBG [20] and 6-methyl-PBG [5], for which the covalently inhibitor-bound HMBS has been reported, a slightly different orientation of the PBG analog in the substrate-binding site may make it difficult to form a covalent bond between the aminomethyl carbon of 2-I-PBG and α-carbon of ring c2, or make the bond unstable.

Catalytic mechanisms of substrate binding and oligopyrrole elongation

Recently, Bung et al. have suggested that stepwise synthesis (oligopyrrole elongation) occurs in HMBS by MD simulations. They showed that the DPM cofactor of the ES_1 and ES_2 intermediates (P3M and P4M in ref. [6]) is retained at the original position found in holo-HMBS and additional PBG molecule(s) are combined to the end of the oligopyrrole chain. In the present crystal structure of 2-I-PBG-bound holo-HMBS, no shift was observed in the DPM cofactor (Figure 3C). This crystal structure appears similar to the MD-simulated ES_1 intermediate structure (P3M) except for the absence of the covalent bond between the cofactor and the inhibitor. However, the present crystal structure of the ES_2 intermediate showed a shift in the DPM cofactor accompanied by the cofactor-binding loop (Figure 4C), in contrast to the MD-simulated ES_2 intermediate structure (P4M). A recent report of the crystal structure of the ES_2 intermediate by Pluta et al. also exhibited such migration of the DPM cofactor compared to that in the holo form [16]. In the present crystal structures, the rings c1 and c2 of the DPM cofactor in the ES_2 intermediate structure, compared to those in the holo-HMBS structure, have little interaction with peripheral residues and the main chain (Table 2).

Our MD simulation of the ES_2 intermediate further showed that basic residues, including those in the lid loop (Lys70 and Lys74), interact intermittently with the acetate/propionate groups of DPM, partially stabilizing the bound DPM. Such a loose binding at the pyrrole-binding sites 3, 4, and 5 may allow oligopyrrole chain shift (Figure 7). Furthermore, the binding of a PBG molecule at the substrate-binding site would cause a large-scale concerted rearrangement of the electrostatic interaction network, as was observed upon ATP binding to a motor protein [59,60], which loosens the electrostatic interactions between the basic residues and PBGs at the pyrrole-binding sites 1 and 2, allowing the shift of the oligopyrrole chain by one pyrrole unit. The open-close motion of the lid loop, which contains lysine residues that interact with the acetate/propionate of PBGs, may have a role in recruiting a PBG molecule to the substrate-binding site and shifting the oligopyrrole chain. As the fluctuation of the insertion region correlates with those of the lid and cofactor-binding loops, the inserting region may enhance the thermal motions of these functional loops.

Based on the present structural data, the following catalytic mechanism is suggested for the initial stage of the HMBS reaction (Figure 8). First, the first PBG molecule binds to the substrate-binding site composed of Arg26, Ser28, Gln34, Ser96, Asp99, Arg167, Asn169, and Arg173 next to the distal pyrrole (c2) of the DPM cofactor (step 1). With the assistance of Gln34 and Asp99, ammonia is eliminated from PBG (step 2). A methylene bridge is formed between the carbon atom of the methylidene group of the deaminated PBG and the α-carbon atom of the distal pyrrole (c2) of DPM (step 3). Along with deprotonation of ring c2, a tripyrrole chain formed of the DPM cofactor and the first PBG molecule moves backward by one pyrrole unit with the cofactor-binding loop (step 4). Then, the second PBG molecule enters the same substrate-binding site, and the oligopyrrole chain elongates and shifts backward to form the ES_2 intermediate. Next, the third PBG molecule binds to the same substrate-binding site of the ES_2 intermediate, a methylene bridge is formed between the

Biochemical Journal (2021) **478** 1023–1042
https://doi.org/10.1042/BCJ20200996

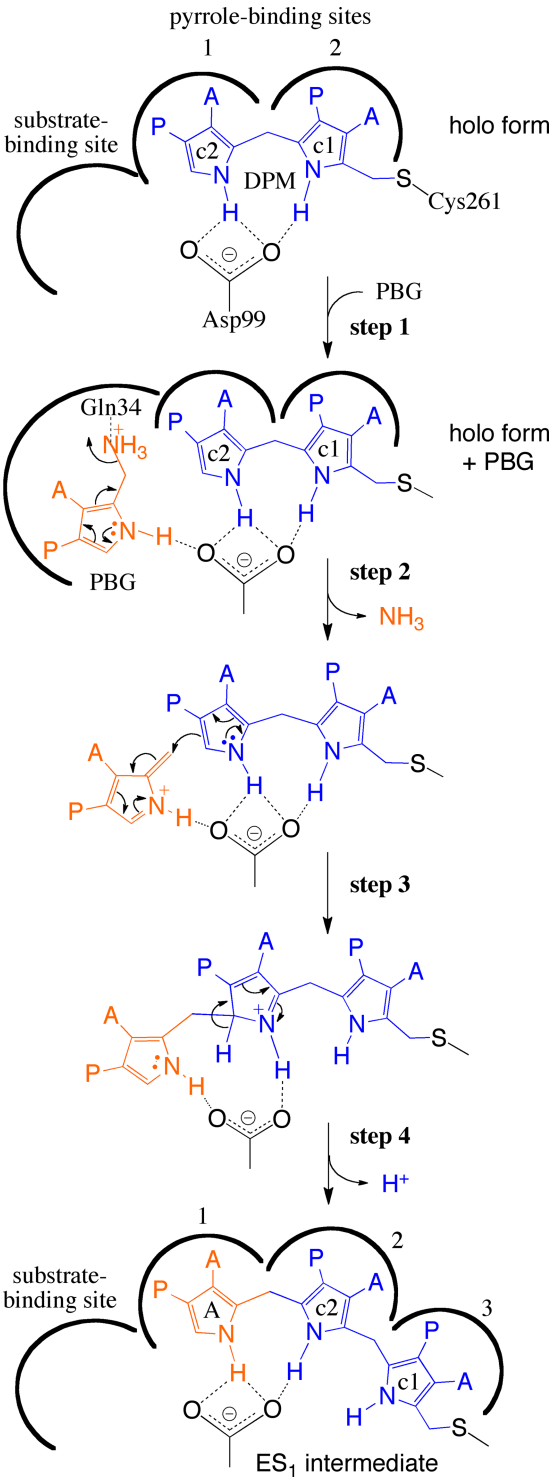

Figure 8. Catalytic mechanism of initial stage of HMBS reaction predicted from the crystal structures complexed with 2-I-PBG.

The acetate and propionate side chains are denoted by –A and –P, respectively. In step 1, PBG binds to a substrate-binding site composed of Arg26, Ser28, Gln34, Ser96, Asp99, Arg167, Asn169, and Arg173. In step 2, Gln34 facilitates deamination of an incoming PBG to form a methylene pyrrolinene intermediate. In step 3, a covalent bond is formed between ring c2 and the intermediate. In step 4, deprotonation of ring c2 and movement of the oligopyrrole chain with the cofactor-binding loop proceeds.

pyrrole ring of PBG and the terminal pyrrole ring B of the tetrapyrrole chain, and the formed pentapyrrole chain moves backward. Further covalent binding of the fourth PBG molecule to the ES_3 intermediate forms an ES_4 intermediate possessing a hexapyrrole chain. Now, no more space would be left for the cofactor-binding loop to move backward because the loop will contact the neighboring α-helix of domain 3. Subsequent cleavage of the hexapyrrole chain in the ES_4 intermediate will produce an HMB leaving holo-HMBS.

HMB release mechanism

To yield HMB, the hexapyrrole chain in the ES_4 intermediate of HMBS must be hydrolyzed at a specific position between pyrroles c2 and A. The 2-I-PBG-bound ES_2 intermediate crystal structure provides some clues about the mechanism of the hydrolysis reaction in the ES_4 intermediate. According to the model suggested by Pluta et al., the ES_3 intermediate has some room behind the cofactor-binding loop including Cys261, so the loop can slide toward domain 3 side by one pyrrole unit [16]. Although they have proposed the involvement of Asp99 in the final dissociation of HMB from the hexapyrrole chain, it is unlikely because Asp99 is far from the rings c2 and A, where the hydrolysis proceeds. On the contrary, in the present structures of the 2-I-PBG-bound and inhibitor-free ES_2 intermediates, >NH of pyrrole c1 in the pyrrole-binding site 4 showed some interaction with the acetate group of pyrrole c2 in the pyrrole-binding site 3 (Figure 7). Given that the substrate-binding site and the pyrrole-binding sites 1–5 accept each pyrrole of the hexapyrrole chain in the ES_4 intermediate, >NH of ring c2 and the acetate group of ring A may interact with each other (Figure 7). The acetate group of ring A, but not the carboxy group of Asp99, may catalyze hexapyrrole chain hydrolysis to form HMB, as shown in Figure 9. In the ES_4 intermediate, the hydrolysis reaction may proceed self-catalytically once the pyrrole N of ring c2 and the acetate group of ring A approach each other due to a conformational change. Furthermore, a cluster of water molecules was observed beside the pyrrole ring c1 and the acetate group of ring c2 in the inhibitor-free ES_2 intermediate structure (Figure 4B), and a water molecule of the cluster may donate

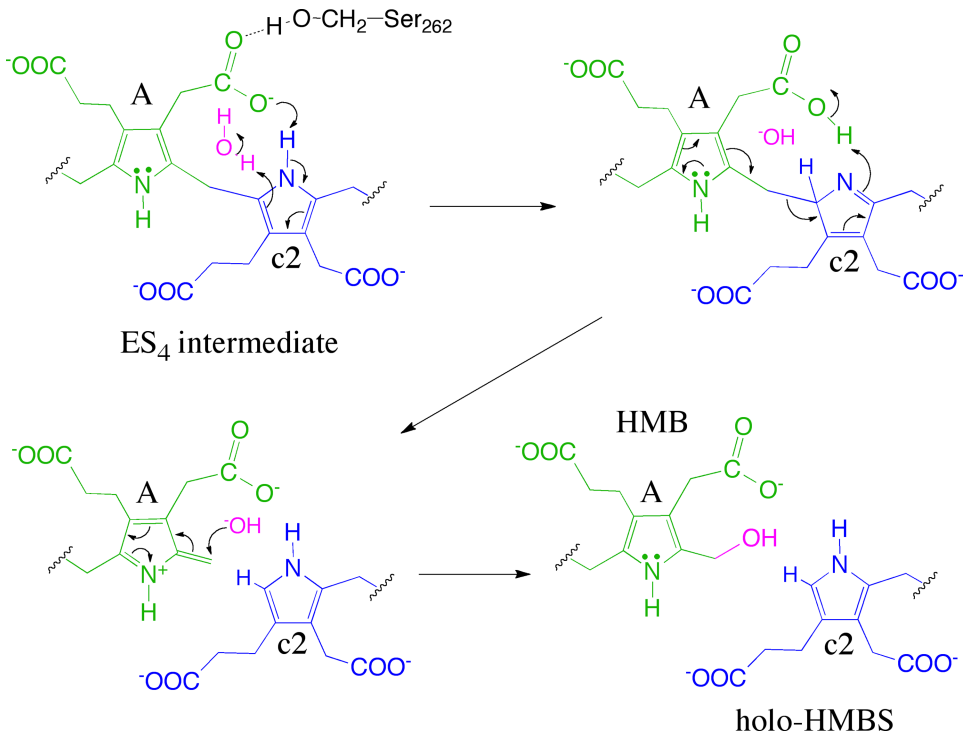

Figure 9. Hypothetical mechanism of dissociation of HMB from the ES_4 intermediate of HMBS.

Pyrroles A and c2 occupy the pyrrole-binding sites 3 and 4, respectively. Parts other than rings A and c2 are omitted for simplicity. First, the acetate group of ring A acts as a general base catalyst to protonate the pyrrole ring c2. Then, the acetate group of ring A acts as a general acid catalyst to cleave the methylene bridge. Finally, hydroxylation of the methylidene group of ring A yields HMB.

Biochemical Journal (2021) 478 1023–1042
https://doi.org/10.1042/BCJ20200996

a proton to initiate the hydrolysis reaction in the ES_4 intermediate. However, hydrolysis of the tetrapyrrole chain could be suppressed because the pyrrole N of ring c2 is stabilized by hydrogen bond with the carbonyl O of Lys98 in the ES_2 intermediate.

Summary

In this work, an enzyme kinetic study of HMBS showed that 2-I-PBG, a derivative of substrate PBG, was a noncompetitive inhibitor ($K_i = 5.4 \pm 0.3$ μM). We determined the crystal structures of holo-HMBS and the ES_2 intermediate in complex with 2-I-PBG, and found that 2-I-PBG was located in the neighborhood of the pyrrole ring c2 of the DPM cofactor and the terminal pyrrole ring B of the tetrapyrrole chain, respectively. To the best of our knowledge, this is the first report of the crystal structure of HMBS complexed with a substrate analog. Since 2-I-PBG is present at the same site in both structures, it is considered that each of the four substrate molecules binds to a single substrate-binding site in HMBS and is condensed consecutively on the DPM cofactor in four successive reactions. Furthermore, MD simulation of the ES_2 intermediate suggested that the thermal fluctuation of the lid and cofactor-binding loops causes substrate binding and migration of the cofactor-containing oligopyrrole chain required for the continuous condensation reaction. The resulting hexapyrrole chain is hydrolyzed self-catalytically to yield HMB.

Data Availability

The coordinates and structure factors of the inhibitor-free and 2-I-PBG-bound holo-HMBS, and the inhibitor-free and 2-I-PBG-bound ES_2 intermediates were deposited in PDB with the accession codes 7CCX, 7CCY, 7CCZ, and 7CD0, respectively. All other data are included in the main article and supplementary materials.

Competing Interests

The authors declare that there are no competing interests associated with the manuscript.

Funding

This work was partly supported by JSPS KAKENHI Grant Numbers 24550201, 15K07018, and 18K05326 to H. S., Grant Number 18H05264 to M. Takano, and grants from the Ishibashi Foundation for the Promotion of Science to H.S.

CRediT Contribution

Hideaki Sato: Conceptualization, Resources, Funding acquisition, Investigation, Visualization, Writing — original draft, Project administration. **Masakazu Sugishima**: Formal analysis, Investigation, Visualization, Writing — original draft. **Mai Tsukaguchi**: Resources, Investigation. **Takahiro Masuko**: Investigation. **Mikuru Iijima**: Formal analysis, Visualization. **Mitsunori Takano**: Formal analysis, Supervision, Funding acquisition, Writing — original draft. **Yoshiaki Omata**: Resources, Writing — review and editing. **Kei Hirabayashi**: Formal analysis, Investigation. **Kei Wada**: Formal analysis, Investigation. **Yoshio Hisaeda**: Supervision. **Ken Yamamoto**: Supervision.

Acknowledgements

We thank Professor Masato Noguchi of Kurume University and Professor Keiichi Fukuyama of Osaka University for helpful discussions at the early stage of this study. We thank Dr. Eiki Yamashita and Dr. Akifumi Higashiura (Present affiliation; Hiroshima University) of Osaka University during diffraction data collection at the BL44XU, SPring-8 (Proposal No. 2016AB6622, 2017AB6725, and 2018A6700). Part of this work was conducted at Kyushu University, supported by the Nanotechnology Platform Program (Molecule and Material Synthesis) of the Ministry of Education, Culture, Sports, Science and Technology (MEXT), Japan. This research was partially supported by the Platform Project for Supporting Drug Discovery and Life Science Research (Basis for Supporting Innovative Drug Discovery and Life Science Research (BINDS)) from the Japan Agency for Medical Research and Development (AMED) under Grant Number JP18am0101072.

Abbreviations

2-I-PBG, 2-iodoporphobilinogen; AIP, acute intermittent porphyria;; DPM, dipyrrolmethane; ES_n intermediate (n = 1, 2, 3, or 4), a reaction intermediate of HMBS possessing an oligopyrrole chain composed of a DPM cofactor and 1, 2, 3, or 4 molecules of PBG, respectively; HMB, hydroxymethylbilane; HMBS, hydroxymethylbilane

synthase; holo-HMBS, a holo form of HMBS with a DPM cofactor; K_i, inhibition constant; MD, molecular dynamics; PBG, porphobilinogen; PDB, Protein Data Bank.

References

1 Grimm, B. (2003) Regulatory mechanisms of eukariotic tetrapyrrole biosynthesis. In *The Porphyrin Handbook,* vol. 12, (Kadish, K.M., Smith, K.M. and Guilard, R., eds.), pp. 1–32, Academic Press, San Diego
2 Layer, G., Reichelt, J., Jahn, D. and Heinz, D.W. (2010) Structure and function of enzymes in heme biosynthesis. *Protein Sci.* **19**, 1137–1161 https://doi.org/10.1002/pro.405
3 Jordan, P.M. (1994) The biosynthesis of uroporphyrinogen III: mechanism of action of porphobilinogen deaminase. In *The Biosynthesis of the Tetrapyrrole Pigments (Ciba Foundation Symposium 180)* (Chadwick, D. and Ackrill, K., eds.), pp. 20–96, Wiley, Chichester
4 Ajioka, R.S., Phillips, J.D. and Kushner, J.P. (2006) Biosynthesis of heme in mammals. *Biochim. Biophys. Acta* **1763**, 723–736 https://doi.org/10.1016/j.bbamcr.2006.05.005
5 Ahmed, R. and Leeper, F.J. (2003) A new synthesis of porphobilinogen analogues, inhibitors of hydroxymethylbilane synthase. *Org. Biomol. Chem.* **1**, 21–23 https://doi.org/10.1039/b209613g
6 Bung, N., Roy, A., Chen, B., Das, D., Pradhan, M., Yasuda, M. et al. (2018) Human hydroxymethylbilane synthase: molecular dynamics of the pyrrole chain elongation identifies step-specific residues that cause AIP. *Proc. Natl. Acad. Sci. U.S.A.* **115**, E4071–E4080 https://doi.org/10.1073/pnas.1719267115
7 Deybach, J.-C. and Puy, H. (2003) Acute intermittent porphyria: from clinical to molecular aspects. In *The Porphyrin Handbook,* vol. 14, chap. 86, (Kadish, K.M., Smith, K.M., Guilard, R., eds.), pp. 23–41, Academic Press, San Diego
8 The Human Gene Mutation Database. http://www.hgmd.cf.ac.uk/ac/gene.php? gene = HMBS
9 Song, G., Li, Y., Cheng, C., Zhao, Y., Gao, A., Zhang, R. et al. (2009) Structural insight into acute intermittent porphyria. *FASEB J.* **23**, 396–404 https://doi.org/10.1096/fj.08-115469
10 Gill, R., Kolstoe, S.E., Mohammed, F., Al D-Bass, A., Mosely, J.E., Sarwar, M. et al. (2009) Structure of human porphobilinogen deaminase at 2.8 Å: the molecular basis of acute intermittent porphyria. *Biochem J.* **420**, 17–25 https://doi.org/10.1042/BJ20082077
11 Louie, G.V., Brownlie, P.D., Lambert, R., Cooper, J.B., Blundell, T.L., Wood, S.P. et al. (1992) Structure of porphobilinogen deaminase reveals a flexible multidomain polymerase with a single catalytic site. *Nature* **359**, 33–39 https://doi.org/10.1038/359033a0
12 Louie, G.V., Brownlie, P.D., Lambert, R., Cooper, J.B., Blundell, T.L., Wood, S.P. et al. (1996) The three-dimensional structure of *Escherichia coli* porphobilinogen deaminase at 1.76-Å resolution. *Proteins* **25**, 48–78 https://doi.org/10.1002/(SICI)1097-0134(199605)25:1<48::AID-PROT5>3.0.CO;2-G
13 Roberts, A., Gill, R., Hussey, R.J., Mikolajek, H., Erskine, P.T., Cooper, J.B. et al. (2013) Insights into the mechanism of pyrrole polymerization catalysed by porphobilinogen deaminase: high-resolution X-ray studies of the *Arabidopsis thaliana* enzyme. *Acta Crystallogr. D Biol. Crystallogr.* **69**, 471–485 https://doi.org/10.1107/S0907444912052134
14 Azim, N., Deery, E., Warren, M.J., Wolfenden, B.A.A., Erskine, P., Cooper, J.B. et al. (2014) Structural evidence for the partially oxidized dipyrromethene and dipyrromethanone forms of the cofactor of porphobilinogen deaminase: structures of the *Bacillus megaterium* enzyme at near-atomic resolution. *Acta Cryst. D Biol Crystallogr* **70**, 744–751 https://doi.org/10.1107/S139900471303294X
15 Uchida, T., Funamizu, T., Chen, M., Tanaka, Y. and Ishimori, K. (2018) Heme binding to porphobilinogen deaminase from *Vibrio cholerae* decelerates the formation of 1-hydroxymethylbilane. *ACS Chem. Biol.* **13**, 750–760 https://doi.org/10.1021/acschembio.7b00934
16 Pluta, P., Roversi, P., Bernardo-Seisdedos, G., Rojas, A.L., Cooper, J.B., Gu, S. et al. (2018) Structural basis of pyrrole polymerization in human porphobilinogen deaminase. *Biochim. Biophys. Acta Gen. Subj.* **1862**, 1948–1955 https://doi.org/10.1016/j.bbagen.2018.06.013
17 Warren, M.J. and Jordan, P.M. (1988) Investigation into the nature of substrate binding to the dipyrromethane cofactor of *Escherichia coli* porphobilinogen deaminase. *Biochemistry* **27**, 9020–9030 https://doi.org/10.1021/bi00425a021
18 Jones, R.M. and Jordan, P.M. (1994) Purification and properties of porphobilinogen deaminase from *Arabidopsis thaliana*. *Biochem. J.* **299**, 895–902 https://doi.org/10.1042/bj2990895
19 Leeper, F.J. and Rock, M. (1996) Interaction of analogues of porphobilinogen with porphobilinogen deaminase. *J. Chem. Soc., Perlin Trans. 1*, 2643–2649 https://doi.org/10.1039/p19960002643
20 Scott, A.I., Roessner, C.A., Stolowich, N.J., Karuso, P., Williams, H.J., Grant, S.K. et al. (1988) Site-directed mutagenesis and high-resolution NMR spectroscopy of the active site of porphobilinogen deaminase. *Biochemistry* **27**, 7984–7990 https://doi.org/10.1021/bi00421a002
21 Wang, J. and Scott, A.I. (1994) Synthesis of the 2-fluoro-11-hydroxy analog of porphobilinogen, a new suicide inhibitor of the enzyme porphobilinogen deaminase. *Tetrahedron* **50**, 6181–6192 https://doi.org/10.1016/S0040-4020(01)80640-2
22 Granick, S. and Bogorad, L. (1953) Porphobilinogen a monopyrrole. *J. Am. Chem. Soc.* **75**, 3610–3610 https://doi.org/10.1021/ja01110a526
23 Omata, Y., Sakamoto, H., Higashimoto, Y., Hayashi, S. and Noguchi, M. (2004) Purification and characterization of human uroporphyrinogen III synthase expressed in *Escherichia coli*. *J. Biochem.* **136**, 211–220 https://doi.org/10.1093/jb/mvh111
24 Hart, G.J., Miller, A.D. and Battersby, A.R. (1988) Evidence that the pyrromethane cofactor of hydroxymethylbilane synthase (porphobilinogen deaminase) is bound through the sulphur atom of a cysteine residue. *Biochem. J.* **252**, 909–912 https://doi.org/10.1042/bj2520909
25 Anderson, P.M. and Desnick, R.J. (1982) Porphobilinogen deaminase: methods and principles of the enzymatic assay. *Enzyme* **28**, 146–157 https://doi.org/10.1159/000459098
26 Rimington, C. (1960) Spectral-absorption coefficients of some porphyrins in the soret-band region. *Biochem. J.* **75**, 620–623 https://doi.org/10.1042/bj0750620
27 Cornish-Bowden, A. (1974) A simple graphical method for determining the inhibition constants of mixed, uncompetitive and non-competitive inhibitors. *Biochem. J.* **137**, 143–144 https://doi.org/10.1042/bj1370143
28 Kabsch, W. (2010) XDS. *Acta Crystallogr. D Biol. Crystallogr.* **66**, 125–132 https://doi.org/10.1107/S0907444909047337
29 Vagin, A. and Teplyakov, A. (1997) MOLREP: an automated program for molecular replacement. *J. Appl. Crystallogr.* **30**, 1022–1025 https://doi.org/10.1107/S0021889897006766

Biochemical Journal (2021) **478** 1023–1042
https://doi.org/10.1042/BCJ20200996

30 Winn, M.D., Ballard, C.C., Cowtan, K.D., Dodson, E.J., Emsley, P., Evans, P.R. et al. (2011) Overview of the CCP4 suite and current developments. *Acta Crystallogr. D Biol. Crystallogr.* **67**, 235–242 https://doi.org/10.1107/S0907444910045749
31 Adams, P.D., Afonine, P.V., Bunkoczi, G., Chen, V.B., Davis, I.W., Echols, N. et al. (2010) PHENIX: a comprehensive python-based system for macromolecular structure solution. *Acta Crystallogr. D Biol. Crystallogr.* **66**, 213–221 https://doi.org/10.1107/S0907444909052925
32 Emsley, P., Lohkamp, B., Scott, W.G. and Cowtan, K. (2010) Features and development of Coot. *Acta Crystallogr. Sect. D Biol. Crystallogr.* **66**, 486–501 https://doi.org/10.1107/S0907444910007493
33 Eswar, N., Webb, B., Marti-Renom, M.A., Madhusudhan, M.S., Eramian, D., Shen, M.Y. et al. (2007) Comparative protein structure modeling using MODELLER. *Curr. Protoc. Protein Sci.* **50**, 2.9.1–2.9.31 https://doi.org/10.1002/0471140864.ps0209s50
34 Gordon, J.C., Myers, J.B., Folta, T., Shoja, V., Heath, L.S. and Onufriev, A. (2005) H++: a server for estimating pK_as and adding missing hydrogens to macromolecules. *Nucleic Acids Res.* **33**, W368–W371 https://doi.org/10.1093/nar/gki464
35 Duan, Y., Wu, C., Chowdhury, S., Lee, M.C., Xiong, G., Zhang, W. et al. (2003) A point-charge force field for molecular mechanics simulations of proteins based on condensed-phase quantum mechanical calculations. *J. Comput. Chem.* **24**, 1999–2012 https://doi.org/10.1002/jcc.10349
36 Jakalian, A., Bush, B.L., Jack, D.B. and Bayly, C.I. (2000) Fast, efficient generation of high-quality atomic charges. AM1-BCC model: I method. *J. Comput. Chem.* **21**, 132–146 https://doi.org/10.1002/(SICI)1096-987X(20000130)21:2<132::AID-JCC5>3.0.CO;2-P
37 Wang, J., Wang, W., Kollman, P.A. and Case, D.A. (2006) Automatic atom type and bond type perception in molecular mechanical calculations. *J. Mol. Graph. Model* **25**, 247–260 https://doi.org/10.1016/j.jmgm.2005.12.005
38 Wang, J., Wolf, R.M., Caldwell, J.W., Kollman, P.A. and Case, D.A. (2004) Development and testing of a genera Amber force field. *J. Comput. Chem.* **25**, 1157–1174 https://doi.org/10.1002/jcc.20035
39 Iijima, M., Ohnuki, J., Sato, T., Sugishima, M. and Takano, M. (2019) Coupling of redox and structural states in cytochrome P450 reductase studied by molecular dynamics simulation. *Sci. Rep.* **9**, 9341 https://doi.org/10.1038/s41598-019-45690-2
40 Case, D.A., *et al.* (2014) *AMBER14,* University of California, San Francisco
41 Gallivan, J.P. and Dougherty, D.A. (1999) Cation-π interactions in structural biology. *Proc. Natl Acad. Sci. U.S.A.* **96**, 9459 https://doi.org/10.1073/pnas.96.17.9459
42 Kauppinen, R., Mustajoki, S., Pihlaja, H., Peltonen, L. and Mustajoki, P. (1995) Acute intermittent porphyria in Finland: 19 mutations in the porphobilinogen deaminase gene. *Hum. Mol. Genet.* **4**, 215–222 https://doi.org/10.1093/hmg/4.2.215
43 Llewellyn, D.H., Whatley, S. and Elder, G.H. (1993) Acute intermittent porphyria caused by an arginine to histidine substitution (R26H) in the cofactor-binding cleft of porphobilinogen deaminase. *Hum. Mol. Genet.* **2**, 1315–1316 https://doi.org/10.1093/hmg/2.8.1315
44 Ulbrichova, D., Hrdinka, M., Saudek, V. and Martasek, P. (2009) Acute intermittent porphyria–impact of mutations found in the hydroxymethylbilane synthase gene on biochemical and enzymatic protein properties. *FEBS J.* **276**, 2106–2115 https://doi.org/10.1111/j.1742-4658.2009.06946.x
45 Lander, M., Pitt, A.R., Alefounder, P.R., Bardy, D., Abell, C. and Battersby, A.R. (1991) Studies on the mechanism of hydroxymethylbilane synthase concerning the role of arginine residues in substrate binding. *Biochem. J.* **275**, 447–452 https://doi.org/10.1042/bj2750447
46 Ong, P.M., Lanyon, W.G., Graham, G., Hift, R.J., Halkett, J., Moore, M.R. et al. (1997) Acute intermittent porphyria: the in vitro expression of mutant hydroxymethylbilane synthase. *Mol. Cell Probes* **11**, 293–296 https://doi.org/10.1006/mcpr.1997.0118
47 Jordan, P.M. and Woodcock, S.C. (1991) Mutagenesis of arginine residues in the catalytic cleft of *Escherichia coli* porphobilinogen deaminase that affects dipyrromethane cofactor assembly and tetrapyrrole chain initiation and elongation. *Biochem. J.* **280**, 445–449 https://doi.org/10.1042/bj2800445
48 Puy, H., Deybach, J.C., Lamoril, J., Robreau, A.M., Da Silva, V., Gouya, L. et al. (1997) Molecular epidemiology and diagnosis of PBG deaminase gene defects in acute intermittent porphyria. *Am. J. Hum. Genet.* **60**, 1373–1383 https://doi.org/10.1086/515455
49 Kauppinen, R. and von und zu Fraunberg, M. (2002) Molecular and biochemical studies of acute intermittent porphyria in 196 patients and their families. *Clin. Chem.* **48**, 1891–1900 https://doi.org/10.1093/clinchem/48.11.1891
50 Lee, J.S. (1991) Molecular genetic investigation of the human porphobilinogen deaminase gene in acute intermittent porphyria. PhD Dissertation. Stockholm: Karolinska Institutet
51 Pischik, E., Mehtälä, S. and Kauppinen, R. (2005) Nine mutations including three novel mutations among Russian patients with acute intermittent porphyria. *Hum. Mutat.* **26**, 496 https://doi.org/10.1002/humu.9381
52 Delfau, M.H., Picat, C., de Rooij, F.W., Hamer, K., Bogard, M., Wilson, J.H. et al. (1990) Two different point G to A mutations in exon 10 of the porphobilinogen deaminase gene are responsible for acute intermittent porphyria. *J. Clin. Invest.* **86**, 1511–1516 https://doi.org/10.1172/JCI114869
53 Shoolingin-Jordan, P.M., Al-Dbass, A., McNeill, L.A., Sarwar, M. and Butler, D. (2003) Human porphobilinogen deaminase mutations in the investigation of the mechanism of dipyrromethane cofactor assembly and tetrapyrrole formation. *Biochem. Soc. Trans.* **31**, 731–735 https://doi.org/10.1042/bst0310731
54 Gu, X.F., de Rooij, F., Voortman, G., Te Velde, K., Nordmann, Y. and Grandchamp, B. (1992) High frequency of mutations in exon 10 of the porphobilinogen deaminase gene in patients with a CRIM-positive subtype of acute intermittent porphyria. *Am. J. Hum. Genet.* **51**, 660–665 PMID: 1496994
55 Floderus, Y., Shoolingin-Jordan, P.M. and Harper, P. (2002) Acute intermittent porphyria in Sweden. Molecular, functional and clinical consequences of some new mutations found in the porphobilinogen deaminase gene. *Clin. Genet.* **62**, 288–297 https://doi.org/10.1034/j.1399-0004.2002.620406.x
56 Deybach, J.C. and Puy, H. (1995) Porphobilinogen deaminase gene structure and molecular defects. *J. Bioenerg. Biomembr.* **27**, 197–205 https://doi.org/10.1007/BF02110034
57 Martinez di Montemuros, F., Di Pierro, E., Biolcati, G., Rocchi, E., Bissolotti, E., Tavazzi, D. et al. (2001) Acute intermittent porphyria: heterogeneity of mutations in the hydroxymethylbilane synthase gene in Italy. *Blood Cells Mol. Dis.* **27**, 961–970 https://doi.org/10.1006/bcmd.2001.0466
58 Woodcock, S.C. and Jordan, P.M. (1994) Evidence for participation of aspartate-84 as a catalytic group at the active site of porphobilinogen deaminase obtained by site-directed mutagenesis of the hemC gene from *Escherichia coli*. *Biochemistry* **33**, 2688–2695 https://doi.org/10.1021/bi00175a043
59 Sato, T., Ohnuki, J. and Takano, M. (2016) Dielectric allostery of protein: response of myosin to ATP binding. *J. Phys. Chem. B* **120**, 13047–13055 https://doi.org/10.1021/acs.jpcb.6b10003
60 Sato, T., Ohnuki, J. and Takano, M. (2017) Long-range coupling between ATP-binding and lever-arm regions in myosin via dielectric allostery. *J. Chem. Phys.* **147**, 215101 https://doi.org/10.1063/1.5004809